BNL 50667

104
9-16-77

LR-1516

SOME RATE AND MODELING STUDIES ON THE USE OF IRON-TITANIUM HYDRIDE AS AN ENERGY STORAGE MEDIUM FOR ELECTRIC UTILITY COMPANIES

GERALD STRICKLAND AND WEN-SHI YU

MASTER

April 26, 1977

BROOKHAVEN NATIONAL LABORATORY
ASSOCIATED UNIVERSITIES, INC.
UNDER CONTRACT NO. EY-76-C-02-0016 WITH THE
UNITED STATES ENERGY RESEARCH AND DEVELOPMENT ADMINISTRATION

DISTRIBUTION OF THIS DOCUMENT IS UNLIMITED

DISCLAIMER

This report was prepared as an account of work sponsored by an agency of the United States Government. Neither the United States Government nor any agency Thereof, nor any of their employees, makes any warranty, express or implied, or assumes any legal liability or responsibility for the accuracy, completeness, or usefulness of any information, apparatus, product, or process disclosed, or represents that its use would not infringe privately owned rights. Reference herein to any specific commercial product, process, or service by trade name, trademark, manufacturer, or otherwise does not necessarily constitute or imply its endorsement, recommendation, or favoring by the United States Government or any agency thereof. The views and opinions of authors expressed herein do not necessarily state or reflect those of the United States Government or any agency thereof.

DISCLAIMER

Portions of this document may be illegible in electronic image products. Images are produced from the best available original document.

BNL 50667
(Energy Storage-
Chemical - TID-4500)

SOME RATE AND MODELING STUDIES ON THE USE OF IRON-TITANIUM HYDRIDE AS AN ENERGY STORAGE MEDIUM FOR ELECTRIC UTILITY COMPANIES

GERALD STRICKLAND AND WEN-SHI YU

April 26, 1977

The work described was supported in part by the Empire State Electric Energy Research Corporation and in part by the United States Research and Development Administration.

NOTICE
This report was prepared as an account of work sponsored by the United States Government. Neither the United States nor the United States Energy Research and Development Administration, nor any of their employees, nor any of their contractors, subcontractors, or their employees, makes any warranty, express or implied, or assumes any legal liability or responsibility for the accuracy, completeness or usefulness of any information, apparatus, product or process disclosed, or represents that its use would not infringe privately owned rights.

DEPARTMENT OF APPLIED SCIENCE
BROOKHAVEN NATIONAL LABORATORY
UPTON, N.Y. 11973

DISTRIBUTION OF THIS DOCUMENT IS UNLIMITED

NOTICE

This report was prepared as an account of work sponsored by the United States Government. Neither the United States nor the United States Energy Research and Development Administration, nor any of their employees, nor any of their contractors, subcontractors, or their employees, makes any warranty, express or implied, or assumes any legal liability or responsibility for the accuracy, completeness or usefulness of any information, apparatus, product or process disclosed, or represents that its use would not infringe privately owned rights.

Printed in the United States of America
Available from
National Technical Information Service
U.S. Department of Commerce
5285 Port Royal Road
Springfield, VA 22161
Price: Printed Copy $4.50; Microfiche $3.00

June 1977 275 copies

TABLE OF CONTENTS

List of Figures

List of Figures - cont'd

List of Tables

Abstract

Dynamic tests and modeling studies were made on the chemical-energy-storage portion of an electrical energy conversion and storage system proposed for leveling the load of an electric utility company. Hydrogen in the form of a metal hydride was used as the energy storage medium. The concept utilizes off-peak power to produce hydrogen by electrolyzing water, storing the hydrogen as iron-titanium hydride, $FeTiH_x$, and subsequently releasing the hydrogen to a fuel cell where the reaction with air generates electrical power. The hydrogen storage portion of the system was tested on a small scale using a 6-in.-diameter test bed about 30-in. long, and containing 84 lb of FeTi alloy. Hydrogen reacts with this alloy at ordinary temperatures, with the release of heat, producing the hydride $FeTiH_x$; and hydrogen is released by heating the hydride to decompose it. The vessel was provided with a water jacket for the use of cold water during hydriding and hot water during dehydriding. In one design, an energy storage system would utilize an array of these hydride containers horizontally mounted in a tank, through which cold and hot water was circulated.

In the six hydriding-dehydriding cycles that were studied, the times that hydrogen flow rates of 40 to 10 standard liters per minute (SLPM) could be sustained was determined. Water temperatures of 30°C (86°F) and 50°C (122°F) were used; and the terminal hydrogen pressures used were 500 psia during hydriding

and ∿16 psia during dehydriding. Under these conditions the dynamic working capacity of the test bed was 1 lb of hydrogen as the composition varied between $FeTiH_{0.175}$ and $FeTiH_{1.400}$. For a 10-hour transfer time the design rating of the unit was 9 SLPM of hydrogen, which is equivalent to 0.119 wt% of the alloy per hour, using water at 80°C (176°F). Temperature profiles and histories were also obtained. A battery comparison test showed that the reserve capacity of the test bed was substantially greater than that expected from the best present-day lead-acid battery in a standard test made at the 50%-discharged condition. In the modeling study it was shown that by using measured values of the bed thermal conductivity and pressure, the analytical and experimental results for hydrogen discharge rate, and amount of hydrogen discharged, were in good agreement. Further studies are required in order to determine the effect of other water temperatures on the dynamic behavior of this test bed.

Introduction

A major problem of distributed electrical energy is that the demand varies throughout the day and week, and there is no universal and cost-effective method of storing large amounts of excess energy when it is available at minimum cost. The cost of producing power to meet peak demands, through the use of peaking facilities to supplement the output of the base-load plant, is much higher than it is when the base-load plant has excess capacity and can thus produce power at minimum cost.[1] Storage of this off-peak power, for use during periods of peak demand, could result in load leveling for electric utility companies. The cost increment provides an economic incentive to develop ways of efficiently storing electrical energy for daily and weekly cycles.

A new and promising load-leveling concept now under development is based on the storage of energy as hydrogen in the form of a decomposable metal hydride. The best known hydride for this application is iron-titanium hydride, $FeTiH_x$; it reacts reversibly with FeTi alloy at ordinary temperatures and has a limiting composition of $FeTiH_2$.[2] In this concept an electrochemical device (electrolyzer), operating on off-peak power, consumes water in producing hydrogen which is stored as $FeTiH_x$; subsequently the hydrogen is released to another electrochemical device (fuel cell) where it reacts with air and generates electrical power to satisfy the peak demand.[1,3,4,5,6] Power-conditioning equipment is also required for the two conversions between alternating and direct current. A practical demonstration of this concept was recently

completed at a power level of 12.5 kW by Public Service Electric and Gas Company of New Jersey. The 10-lb hydrogen storage unit was designed and constructed for PSE&G by BNL under a shared-cost agreement.[4,5,7]

There are several advantages to storing energy in the form of $FeTiH_x$. Its use avoids the high pressure of compressed-gas storage, or the low temperature of hydrogen stored as a liquid. Iron-titanium hydride can sustain thousands of storage cycles when utilizing the high-purity hydrogen from electrolyzers--without any gradual loss such as the slow boil-off from liquid hydrogen.[8] Another advantage possessed by this method of storing energy is that it is environmentally attractive. In addition to the source of electrical power, the only other service required is a water supply. Water is the source of hydrogen, and cold water is used for removing the heat released during hydriding; the hot water required during dehydriding is obtained from the fuel cell when the two reactants, hydrogen and oxygen (from air), combine to form water as electrical power is being generated. Thus this energy storage concept demands little from the environment and it has no detrimental effect on the environment. A secondary benefit can be realized through use of the by-product oxygen for secondary wastewater treatment.

In particular, the work described here is limited to the energy-storage portion of the system. The rates at which hydrogen can be stored in and released from a 6-inch-diameter hydride container were determined for one set of water conditions.[9] An

energy storage system would utilize an array of these containers horizontally mounted in a tank provided with circulating cold and hot water. A modeling study was also made for use in the prediction of performance; similar studies have been made.[10]

The above effort is part of the Hydrogen Technology Development Program supported by the U.S. Energy Research and Development Administration. A substantial portion of the funding required for the energy storage work was contributed by the Empire State Electric Energy Research Corporation (ESEERCO), a group of eight utilities sponsoring energy research and development work in New York State. Specifically, ESEERCO funding was used for the design, fabrication and operation of a 6-in.-diameter, hydrogen-storage test bed, and for the associated process equipment and instrumentation. This report describes the results of the numerous tests performed with the ESEERCO Test Bed, which represents a heat-transfer cell of the external-fluid type. ESEERCO funding also covered data evaluation and development of the mathematical model used to describe the thermal and mass-transfer behavior of the test bed.

The results of the work performed in this cooperative program have provided information useful in the design of larger storage units. One removable internal assembly proposed for a 2-ft-diameter unit now being designed will have an annular test bed with a water jacket on the minor diameter; it will supplement the water jacket on the vessel exterior. Other proposed removable assemblies will employ water tubes or embossed heat-transfer panels. At the

conclusion of this next test program, an assessment will be made, and the preferred design will be utilized for the next storage device. Before passing on to the new work, several more runs will be made with the ESEERCO Test Bed at the 50% discharged condition, for further comparison with the performance of the best present-day lead-acid battery. The goal of the continuing Hydrogen Technology Development Program is to develop cost-effective materials and equipment, so that the proposed system can provide a practical method of storing electrical energy. The ESEERCO Test Bed has been a vital part of that program.

Hydride Behavior

The ability of hydrogen to react with certain metals and alloys to form decomposable hydrides is the basis for this method of energy storage. These materials readily take up or release hydrogen, depending upon the temperature and pressure of the system. The choice of hydride depends upon the application. For large-scale land-based applications, the leading contender at this time is iron-titanium hydride, $FeTiH_x$, where x approaches a value of two under equilibrium conditions when materials of very-high purity are used. Details on the formation and properties of this material have been described by Reilly & Wiswall.[2] The advantages of $FeTiH_x$ are that it can react with and release hydrogen at ordinary temperatures, and that potentially FeTi alloy, from which $FeTiH_x$ is prepared, can be produced cost-effectively from the ore ilmenite ($FeTiO_3$) which is very abundant. The alloy is used in granular form. An activation procedure is necessary in preparing $FeTiH_x$ because the initial reaction rate is slow. The first step consists of heating and evacuation in order to outgas the surfaces. Low pressure flushing with hydrogen helps, and also initiates the reaction which is continued at moderate pressure ($\sim$500 psia) after cooling the material to essentially room temperature. This contact with hydrogen causes severe embrittlement and the development of microfissures which greatly increase the surface area and reactivity of the material. Volumetric expansion during the

reaction with hydrogen also contributes to attrition of the particles. Activation can be aided by hydriding and dehydriding the material every day or two; the amount of hydrogen stored increases with each cycle until full capacity is reached. High-purity alloy requires up to two weeks to become fully activated, whereas material containing several tenths of a percent of oxygen (as oxides) can be activated in considerably less time--at the expense of reduced hydrogen storage capacity.[11,12]

The basic reaction which occurs with high-purity materials may be summarized as follows:

$$1.08\ FeTiH_{0.1} \rightleftarrows 1.08\ FeTiH_{1.95}. \qquad (1)$$

In practical systems the hydrogen content, H_x ranges from approximately $H_{0.2}$ to $H_{1.4}$, and the working range is expressed as $\Delta H_x = 1.2$. Over this range the thermal load is close to 6250 Btu/lb H_2 (7 Kcal/gram mole). Heat must be removed in the forward reaction (hydriding, charging or association), and it must be supplied during the reverse reaction (dehydriding, discharging or dissociation). The reaction rate is governed by the rate of heat transfer, and is also limited by the comparatively low thermal conductivity of the $FeTiH_x$ bed. During hydriding the system pressure must exceed the equilibrium association pressure of the hydride in order for the reaction to proceed, and likewise during dehydriding the dissociation pressure must exceed the pressure of the system that hydrogen is discharging to.

A demanding requirement of $FeTiH_x$ is that it requires hydrogen having a purity of $\geq$99.999%. It is sensitive to the presence of oxygen, and as little as 10 ppm will cause a slow loss of storage capacity.[13] Thus hydrogen which is produced electrolytically for this use is purified by reacting it with the residual oxygen, in a catalytic reactor, and the water formed is removed by a drying agent.

The equilibrium between a decomposable hydride and hydrogen is described by a plot of pressure versus composition for a given temperature. This relationship is shown in Figure 1 for hydride produced from zone-refined Fe and Ti[2]; the characteristics of the $FeTiH_x$ used in the present work closely approximate those illustrated. The FeTi alloy was one of two batches produced by Titanium Metals Corp., a Division of N.L. Industries. Testing showed that the second batch, designated NL-2, had a higher storage capacity, presumably because of its lower oxygen content; so it was selected. In the pressure-composition plot the upper curve is for the forward reaction in which hydrogen is stored, and the lower curve is for the reverse reaction in which hydrogen is released. Hydride composition is expressed as the atom ratio of hydrogen to metal, H/M. Thus for the limiting composition, $FeTiH_2$, H = 2 and M = 1+1; therefore H/M = 2/2 = 1, the highest value of the abscissa. In other words, at any point the value of x is twice that of H/M. The pressure difference between the curves is due to hysteresis, a phenomenon which is not clearly understood. Its effect is that hydrogen

is released at a lower pressure than is required to store hydrogen. The steep initial rise in pressure is the region of solid solution of hydrogen in the metal lattice; the plateau is the region of FeTi and $FeTiH_1$; and the subsequent rise is the region of $FeTiH_1$ and $FeTiH_2$. Increasing the system temperature causes the hydrogen pressure to increase, and is illustrated by the isotherms shown in Reference 2.

Description of Equipment and Operation

The hydriding and dehydriding reactions require an atmosphere of high-purity hydrogen and a means of handling the thermal load in order to be sustained. This need is satisfied through the use of a closed container (pressure vessel) provided with a heat exchanger. Such a vessel is called a hydride reservoir; experimental units are generally referred to as test beds. The unit used for this work was named the ESEERCO Test Bed. A reservoir also requires a particle barrier, or filter, to retain the fine particles produced by attrition. Connections for the transfer of hydrogen and for temperature and pressure sensors are also needed. The heat exchanger may be immersed in the bed or it may be in the form of a water jacket or its equivalent. They are classified as internal and external types, respectively, and both rely on thermal conduction in the hydride. Each type can be considered as a unit heat-transfer cell; namely, as a cylinder having a water tube on its axis or as a cylinder having water on its external surface.

The ESEERCO Test Bed was conceived as a cylindrical heat-transfer cell having a water jacket and a porous-metal tube (PMT) on its longitudinal axis; thus both the heat and hydrogen flows are radial. In this concept the required number of hydride containers would be arranged horizontally in a tank provided with circulating water. The external-fluid type of heat-transfer cell has an apparent advantage in that the heat-transport fluid, water

in this case, is adjacent to the major part of the cross-sectional area of the bed. The water tank is not a pressure vessel, and the hydride containers are small-diameter pressure vessels. A cell diameter of 6 inches was selected for the ESEERCO Test Bed on the basis of experience obtained with the 3-inch-diameter, internal-fluid-type of cell used in the 10-lb hydrogen reservoir constructed for Public Service Electric and Gas Company of New Jersey. In comparing the geometric factors involved in these two types of cells, it was judged that a 6-inch-diameter cell of the external-fluid-type would approach the performance of the 3-inch-diameter internal-fluid-type of cell.

The vessel was made from 6-in. schedule 10 pipe, (0.134-inch nominal wall thickness) welded to two end caps, and the bottom cap was provided with a baffle plate to support the bed. A sketch of the test bed without its removable water jacket is shown in Figure 2 and the vessel components are shown in Figure 3. All of the structural components were made of type 316 stainless steel. A 5/8-in.-O.D. PMT was used as the particle barrier; this material has a filtration rating of 0.5 μM (micron) and a wall thickness of 1/16 in. The fixture for supporting the thermocouples was attached to the top cap, and the completed assembly is shown in Figure 4. Twenty-one thermocouples were provided for measuring internal temperatures both radially and axially. Their general arrangement is shown in the test bed sketch and their specific locations are listed in Table 1. The

three radial positions were 120° apart; and thermocouples were located at 0, 25, 50 and 87.5% of the net cross-sectional area (CSA). Iron-Constantan thermocouples having 1/16-in.-O.D. sheaths of stainless steel were installed in groups of three, passing through Teflon seals.

A photograph of the completed vessel beside its water jacket is shown in Figure 5, and the test bed may be seen on its stand in Figure 6. The vessel was designed in accordance with the ASME Code, Section VIII Division 1, Pressure Vessels. Its design pressure was 633 psig and the hydrostatic test pressure was 950 psig. All major welds were X-Rayed and found satisfactory. Subsequently, the vessel passed a helium leak test.

In preparation for the experimental program, the FeTi alloy was broken up into 1- to 1.5-in. lumps and then ground and sized at BNL. Except for the 2% of fines which passed through a 100-mesh sieve, the material was used as ground; the largest particles allowed were those that passed through a 4-mesh sieve. Figure 7 is a full-scale picture of alloy having this range of particle sizes, the range being designated as -4 + 100 mesh size. A loosely-packed bed of the 84 lb of alloy used was obtained by rolling the vessel around its longitudinal axis and then carefully standing it up. At this time the void space was 47%, and it was estimated that bed depth would increase to about four diameters as a result of the 15% volumetric expansion expected upon conversion to the hydride. The particle size distribution of the

alloy is given in Table 2, and the results of the chemical analysis are provided in Table 3. Its oxygen content was 620 PPM, an acceptable level.

The activation step, in which the FeTi alloy was converted to the hydride, was started by heating the test bed (without its jacket) to nearly 600°F (315°C) under vacuum. During this period the bed was flushed with hydrogen several times. For this operation the vessel was wrapped with heating cable and insulation; it was supported by the skirt rings resting on two sets of rollers so that it could be occasionally oscillated about its horizontal axis and kept loosely packed. Subsequently hydrogen was admitted at 30 psia and the test bed was allowed to cool with the insulation removed. On the following day the charging pressure was increased to 500 psia and the reaction was allowed to continue for three days before the reservoir was heated to 600°F and evacuated. After twelve daily hydride-dehydride cycles, the material reached 92% of its dynamic working capacity which was later found to be 1 lb of hydrogen. Although the activation step is time consuming, it is necessary only initially. If the hydride should become contaminated either through the use of impure hydrogen or the admission of air or water vapor to the system, its storage capacity can be restored by reactivation under conditions similar to those used initially.

The equipment flow diagram for the system is shown in Figure 8. Most of the components also appear in Figure 9 which

shows the instrument and control panel boards. The water tank, pump and associated equipment, as well as the test bed are located between the panel boards. All of the valves normally operated, the pressure regulator, and the pressure gauges were mounted on the front of the control panel board. The thermal mass flowmeters were mounted behind it. During hydriding the flow path was through valves 6, 4 and/or 17, 7, 2 and 1; and during dehydriding the path was through valves 1, 2, 3, 4 and/or 17 and 5. The vessel and its contents were protected by a rupture disc, rated to burst at 635 psia, and a relief valve which opened at 560 psia. This valve was used to prevent any entry of air in event of a disc rupture. The normally-open excess flow valve served to keep the discharge side of the disc at atmospheric pressure; in event of a rupture it would close. The vent line was also provided with a check valve (not shown) to prevent entry of air whenever hydrogen was released. In the closed-loop water system, the tank temperature was maintained at the desired value by controlling the amount of make-up cold or hot water, and the equivalent volume flowed to the drain.

The instrument panel was provided with digital and analog data acquisition instruments. Hydrogen pressure, flow rate, integrated flow, $FeTiH_x$ temperatures, water inlet and outlet temperatures, as well as the time and date, were recorded in digital form. A selector switch was provided for recording this data at intervals ranging from 1 to 16 minutes. The hydrogen pressure was also recorded directly so that the pressure trend

was always visible. During hydriding the regulated pressure was kept 25-75 psi higher than the reservoir pressure, by manual advancement of the pressure regulator, in order to ease manual control of the hydrogen flow rate. Control was considerably more difficult during the early stage of dehydriding because of the high pressure drop across the valve.

The first dehydriding operation was performed when it was concluded that sufficient time had been allowed for activation. Hydrogen was discharged during three operating periods until the bed pressure decreased to 19 psia. The amount released, 1.19 lb, was in excess of the dynamic operating amount because of the long charging time used during activation. After another hydride-dehydride cycle, the flowmeter throttling valves were replaced with micrometer needle valves in order to improve flow control. Several compression-type tube fitting joints were also changed to welded construction. The above runs made during the first two cycles provided training for the operators and a final check-out of the system.

Experimental Results and Discussion

The first formal series of runs was made for the purpose of determining the length of time that various hydrogen flow rates could be sustained for both parts of the cycle. Water was circulated through the jacket at 2 GPM and 30°C (86°F) during hydriding, and at 50°C (122°F) during dehydriding. The hydrogen flow rates studied were 40, 30, 25, 15 and 10 standard liters per minute (SLPM, at 14.7 psia and 20°C (68°F)). In each case, operation was continued until 1 lb (5409 liters) of hydrogen was transferred. The limiting pressures for hydriding and dehydriding were 500 psia, and approximately 16 psia, respectively. For the charging half of the cycle these times ranged from 72 to 519 minutes, and for the discharging half they were 79-510 minutes. This variation in the time of sustained flow rate for each half of the cycle is shown in Figures 10 and 11, along with the amount of hydrogen transferred. The lower curves show that lower flow rates can be sustained for longer times, and the upper curves show the total amount of hydrogen transferred for the time of sustained flow rate. For example, the charging rate of 30 SLPM was sustained for 115 minutes (lower curve), and for this time 0.65 lb of hydrogen was transferred (upper curve). All of the flow data for this series of runs is listed in Table 4. Parts of cycles 3, 4 and 5 were performed in more than one operation after the time for each sustained flow rate was obtained. The dynamic composition range was close to $FeTiH_{0.175}$ - $FeTiH_{1.400}$;

thus ΔH_x = 1.225 for the above operating conditions.

All of the above data obtained for the third (E03) are shown in plotted form in Figures 12 through 17. As seen from Figure 12 and Table 4, the charging flow rate of 40 SLPM in Run E03C1 was maintained for 72 minutes, at which time the desired pressure of 500 psia was attained and 0.532 lb of H_2 was charged. The flow rate rapidly decreased, and when one of the flowmeters was turned off, there was a small step change in the rate. During recalibration of the flowmeters it was found that their errors were in opposing directions. An average of the flow rate values was plotted during the time of sustained flow rate; thereafter the instantaneous flow rates were used. The decrease in reservoir pressure after the end of hydrogen flow was due to continued hydriding. Subsequently hydrogen was charged for an additional 84 minutes until the total amount was 0.999 lb. In Run E03D1 the flow rate of 40 SLPM was maintained for 75 minutes, and 0.579 lb of H_2 was discharged. Subsequently, the test bed pressure recovered enough to discharge more hydrogen, and the total amount released was 1.057 lb.

The temperature measurements made during the third cycle at mid-height of the bed are plotted as temperature profiles in Figures 14 and 15, and as temperature history in Figures 16 and 17. In each case the temperature value plotted is the average of three readings taken from thermocouples 120° apart; and for any group of three, the values were always within a range of 3°C

(5.4°F). The profiles during charging (Figure 14) showed that the maximum temperature occurred essentially when 500 psia was reached and the flow rate started to decrease below 40 SLPM. During the first 73 minutes of rising temperature profiles, the maximum temperatures were located close to the 18% line of the cross-sectional area. The lower temperature at the PMT was due to the cooling effect of the incoming hydrogen; this effect diminished as the flow rate decreased. At the vessel wall the temperatures converged at approximately 30°C (86°F), the temperature of water flowing along the outer wall of the vessel. A similar set of profiles for the discharging half of the cycle is shown in Figure 15. When the flow rate could not be sustained at 40 SLPM, after 79 minutes of operation, the temperature was close to being the minimum value measured. Bed temperatures during charging are plotted as a function of time in Figure 16. Practically all of the temperatures decreased as soon as the flow rate began to fall below 40 SLPM at the end of 72 minutes. There was some difficulty in maintaining the water temperature at 30°C here, and somewhat more difficulty in maintaining the water at 50°C (122°C) during discharging (Figure 17). The latter variations were caused by large temperature changes in the hot water supply, and the effect of these variations was evident to at least the 87.5% - CSA zone.

All of the remaining data obtained on the time variation of reservoir pressure, flow rate and amount of hydrogen transferred,

for cycles E04 through E08, are plotted in Figures 18 through 27. Discussion of the results will be limited to those for cycle E08, including the temperature histories and profiles, because the flow rate of 10 SLPM is close to being the 10-hour rating of this test bed for the electric-utility application. In the charging run (E08C1) the flow rate was sustained for 519 minutes (8.65 HR), at which time the test-bed pressure reached 500 psia; thereafter the flow rate decreased very rapidly, at first, and then gradually to a final value of 3.61 SLPM. When the hydrogen supply was turned off, the bed pressure began to decrease toward the equilibrium association value as hydrogen in the gas phase continued to react with the cooling hydride at the bed interior. The curve for pressure shows, at any time, the value necessary to maintain the flow rate. In the discharging run (E08D1) the flow rate was sustained for 510 minutes (8.50 HR), by which time the pressure had decreased to 18 psia. The bed pressure began to recover toward the equilibrium value after flow was stopped. As mentioned previously, extrapolation of the rate data showed that, for the water temperatures and terminal pressures used, the ESEERCO Test Bed could sustain a flow rate of close to 9 SLPM for each 10-hour part of the cycle. This rate is equivalent to 1.19×10^{-3} gram H_2/Hr-gram FeTi alloy, or 1.19×10^{-3} lb H_2/Hr lb FeTi alloy, over the composition range $FeTiH_{0.175}$ - $FeTiH_{1.400}$.

Curves of the temperature history for both parts of the cycle are shown in Figures 28 and 29. In each case the inner 50% of the bed went through a temperature wave during the period of constant flow rate. Several factors contributing to this shape are mentioned below; however, others may be involved. At the start of hydriding the bed is essentially isothermal and the incoming hydrogen begins to react throughout the bed. The inner bed material, being farther away from the coolant, increases more rapidly in temperature, as shown in Figure 28. These gradients increase as the reaction proceeds. The reaction occurs in the bed wherever the charging pressure exceeds the equilibrium association pressure for that local bed temperature. Thus, where the temperature is increasing more rapidly, the reaction rate decelerates and causes the temperature to begin leveling off as dynamic equilibrium is approached. The temperature data show that the reaction zone proceeds inwardly (toward 0% CSA). Because bed material at the inner zones has become higher in temperature, it doesn't resume reacting until the pressure becomes moderately high and again exceeds the equilibrium association pressure. Then as this material reacts, its temperature rises again because it is farther from the coolant. One factor contributing to the temperature trough is that the thermal conductivity of the hydride increases as the pressure increases; thus lower temperatures (lower Δt's) are satisfactory for transfer of heat to the coolant. Likewise part of the final rise in temperature is due to an

increase in heat release as more of the bed material is converted from the monohydride to the dihydride.

The shape of the temperature-history curve for the discharge part of the cycle is similar to the previous curve, but is inverted because heat must be added to the system. At the start of dehydriding the bed is essentially isothermal and some hydrogen is released throughout the bed along with the free gas. The inner bed material, being farther away from the hot water in the jacket, decreases more rapidly in temperature, as shown in Figure 29. These gradients increase as the reaction proceeds. The reaction occurs in the bed wherever the equilibrium dissociation pressure for that local bed temperature exceeds the pressure in the test bed. The initial temperature gradients are lower than during charging because the thermal conductivity is higher at the pressures involved. One factor contributing to the temperature trough is that less heat is required as the dihydride content of the bed decreases. Part of the final decrease in temperature is due to further reduction in thermal conductivity at low pressure. The temperature profiles in the bed are shown in Figures 30 and 31 for both parts of the cycle. As is evident in the temperature-history curves, the temperature gradients are greatest at the end of the sustained-flow-rate period. The difference in these two gradients is mainly due to the substantial differences in thermal conductivity of the bed. A better understanding of $FeTiH_x$ behavior will be possible when more detailed pressure-temperature-composition data are available.

Some additional useful information was obtained from two of the other runs completed after the contract period ended. Run E10D1 was made at 9 SLPM in order to determine if this rate could be sustained for 10 hours. The initial water temperature was slightly less than 70°C (158°F), and it was gradually increased to 80°C (176°F) over the next 2.5 hours. As expected, the entire 1 lb of hydrogen was released at 9 SLPM. The terminal pressure was 45 psia, and 0.935 lb was transferred before the pressure fell below 100 psia. Under these dynamic conditions the 1 lb of hydrogen released was ∿83% of that estimated from the equilibrium data.

In the other run, the ESEERCO Test Bed was compared with the best present-day lead-acid battery in a standard discharge test. In a 15-second test made with a battery at the 50% discharge point, its expected rating is 130 W/kg.[14] Although the test-bed rating was limited by the flowmeter range, it was determined that the battery rating (at 100% efficiency) could be sustained for 31 minutes using heating water at 80°C. Thus the test bed has considerably more reserve capacity than the battery in this discharge test.

Modeling Studies

Some work was done on modeling in order to examine the dynamic behavior of a hydride bed and establish the effect of system variables on the hydriding and dehydriding rates. These results will be used in optimizing the design of larger units. In the present conduction-bed model, heat is transferred across the containment wall; a variation of this class of beds is one having heat-exchanger tubes in the bed. A thermal advantage of the present configuration is that the heat-transport fluid is adjacent to the major part of the cross-sectional area of the bed. The thermal conductivity value used for the bed was one obtained by measurement; a value considered representative for the operating pressure range was selected. Thus the value is an effective one and is comprised of the particle, interparticle and hydrogen conductivities. The analytical procedures involved solving the energy and mass balance equations given below:

$$k \frac{\partial^2 T}{\partial z^2} + k\left(\frac{\partial^2 T}{\partial r^2} + \frac{1}{r}\frac{\partial T}{\partial r}\right) - (1-\varepsilon)\phi\Delta H = (1-\varepsilon)\rho C_p \frac{\partial T}{\partial t} , \qquad (2)$$

and

$$\frac{d(H/M)}{dt} = \frac{-\phi}{\rho}\frac{MW}{N} , \qquad (3)$$

where

$$\phi = f(T, H/M, P) . \qquad (4)$$

The temperature and composition solutions of these equations were sought by the method of finite differences, using a CDC 6600 computer, for the following boundary conditions:

$$-k \frac{\partial T}{\partial r} = h(T-T_b) \qquad \text{at } r = r_1 \qquad (5)$$

$$\frac{\partial T}{\partial r} = 0 \qquad r = r_2 \qquad (6)$$

$$\frac{\partial T}{\partial z} = 0 \qquad z = 0, Z, \qquad (7)$$

where

k = effective thermal conductivity of hydride bed, 1.0 Btu/hr-ft^2-^{o}F

T = bed temperature, ^{o}F

T_b = average temperature of water, ^{o}F

z = axial coordinate, ft

r = radial coordinate, ft

ε = void fraction in bed

ϕ = reaction rate, lb H_2/hr-ft^3

ΔH = heat of reaction Btu/lb H_2

h = heat transfer coefficient, Btu/hr-ft^2-^{o}F

ρ = hydride density, lb/ft^3

C_p = hydride heat capacity, Btu/lb-^{o}F

t = time, hr

H/M = ratio of hydrogen atoms to metal atoms for a given hydride

MW = molecular weight of the hydride, lb/lb mole

N = number of metal atoms per "molecule" of a given hydride

P = pressure, atm

Z = length of the hydride bed, ft.

In order to achieve the constant discharge rate, a linear decreasing external pressure variation, obtained from the experimental data, was used as an input. The main outputs from the model were the hydrogen charging and discharging rates of the system and the temperature profiles in the bed. Good agreement was obtained between the experimental and analytical rate data, as shown in Figure 32 for Run E08D1. In comparing the analytical temperature profiles, shown in Figure 33, it is evident that the agreement was good only at the end of the period of sustained hydrogen flow rate. The profiles for 240 minutes differed by 6°C (10.8°F), with the test bed being higher in temperature. At 132 minutes the profiles differed considerably; the measured bed temperature steadily decreased toward 0% CSA, and the analytical profile was somewhat higher and essentially flat for the inner half of the bed. Some improvement in the results can be made by using pressure-dependent thermal-conductivity values instead of one fixed value.

Conclusions

A small test bed of iron-titanium hydride ($FeTiH_x$) was used in determining how hydride containers would function as part of an energy storage system that could be used by an electric utility company in leveling its load. The rates at which high-purity hydrogen could be stored or released from the energy storage medium, $FeTiH_x$, represent the rates at which off-peak power could be used to produce hydrogen by the electrolysis of water, and the rates at which hydrogen could be utilized in a fuel cell to generate power for satisfying a peak demand.

It was determined that the maximum hydrogen storage capacity, under the operating conditions studied, was 1.19 wt% of the FeTi alloy, and that a uniform hydrogen flow rate of 9 standard liters per minute (0.32 SCFM) could be sustained for a 10-hour transfer period.

The modeling studies showed that good agreement could be obtained with the experimental values for flow rate and amount of hydrogen discharged. A limitation of the computer program at this stage of development is that the pressure history must be used as an input. Without this information the model can be used to predict behavior under other conditions, but the results will be relative instead of absolute.

The storage device performed as expected and was easy to operate. It was also demonstrated that this test bed has a substantially higher reserve capacity than the best lead-acid battery at the 50%-discharge condition.

Acknowledgement

The authors express their appreciation to J. J. Reilly and J. R. Johnson for helpful discussions on hydride behavior, to M. J. Rosso for assisting with some of the operation, and to F. J. Salzano for his guidance during the course of the program. The authors are also grateful to J. Fedelem, J. Hala, W. Johnson, W. Lewis, A. Wolke, and A. Wood for their efforts in fabrication and assembly of the equipment; to C. Davis, J. Loper, and G. Schoener for their efforts in providing and servicing the instrumentation; to J. Fedelem and W. Lewis for assisting in operation of the equipment; to E. Saunders and A. Epple for processing of the data; and to B. Ivero for typing the manuscript. We also acknowledge the financial contribution made by Empire State Electric Energy Research Corporation toward the total cost of building and operating the test bed and its associated equipment.

REFERENCES

1. Casazza, J. A., Huse, R. A., Sulzberger, V. T., Salzano, F. J. Possibilities for Integration of Electric, Gas, and Hydrogen Energy Systems. International Conference on Large High Voltage Electric Systems, Paris, France, August 21-29, 1974.

2. Reilly, J. J., Wiswall, Jr., R. H. The Formation and Properties of Iron Titanium Hydride. Inorg. Chem., 13 218, (1974).

3. Salzano, F. J., Cherniavsky, E. A., Isler, R. J., Hoffman, K. C. On the Role of Hydrogen in Electric Energy Storage. Hydrogen Energy Part B, p. 915-932, T. Nejat Veziroglu, Ed., Plenum Press (1975).

4. Strickland, G., Reilly, J. J., Wiswall, Jr., R. H.,. An Engineering-Scale Energy Storage Reservoir of Iron Titanium Hydride. Hydrogen Energy Part A, p. 611-620, T. Nejat Veziroglu, Ed., Plenum Press (1975).

5. Burger, J. M., Lewis, Peter A., Isler, R. J., Salzano, F. J. Energy Storage for Utilities via Hydrogen Systems. 9th Intersociety Energy Conversion Engineering Conference, San Francisco, California, August 26-30, 1974.

6. Fernandes, R. A. Hydrogen Cycle Peak-Shaving for Electric Utilities. 9th Intersociety Energy Conversion Engineering Conference, San Francisco, California, August 26-30, 1974.

7. Strickland, G., Reilly, J. J. Operating Manual for the PSE&G Hydrogen Reservoir Containing Iron Titanium Hydride. BNL 50421. February 1974.

8. Salzano, F. J., Project Manager. Hydrogen Production and Storage in Utility Systems, Semiannual Progress Report, July 1, 1975 to December 31, 1975. BNL 50590. January 1976.

9. Strickland, G., Milau, J., Yu, Wen-Shi. The Behavior of Iron Titanium Hydride Test Beds: Long Term Effects, Heat Transfer and Modeling. First World Hydrogen Energy Conference, Miami Beach, Florida, March 1-3, 1976. BNL 20876.

10. Yu, Wen-Shi, Suuberg, E., Waide, C. H. Modeling Studies of Fixed-Bed Metal-Hydride Storage Systems. Hydrogen Energy Part A, p. 621-643, T. Nejat Veziroglu, Ed., Plenum Press (1975).

11. Reilly, J. J., Johnson, J. R. Titanium Alloy Hydrides, Their Properties and Applications. BNL 20791. December 1975. First World Hydrogen Energy Conference, Miami Beach, Florida, March 1-3, 1976.

12. Sandrock, G. D., Reilly, J. J., Johnson, J. R. Metallurgical Considerations in the Production and Use of FeTi Alloys for Hydrogen Storage. Proc. 11th Intersociety Energy Conversion Engineering Conference, 1976, p. 965-971.

13. Salzano, F. J., Project Manager. Hydrogen Production and Storage in Utility Systems, Annual Progress Report, January 1, 1976 to September 30, 1976. BNL 50631. In press.

14. ERDA National Laboratories Study Group, L. G. O'Connell. The Role of Energy Storage Power Systems in Transportation--Status Report, Volume II, Storage Device and Power Systems Evaluation. LLL UCID-17274. September 30, 1976.

Table 1

ESEERCO TEST-BED THERMOCOUPLE LOCATIONS

TC No.	Elevation, in.[a]	% CSA[b]	Angle, Degrees[c]
1, 2, 3	3.19	50	0, 120, 240
4, 5, 6	5.0	100	60, 180, 300
7, 11, 15	12.75	0	60, 180, 300
8, 12, 16	12.75	25	60, 180, 300
9, 13, 17	12.75	50	60, 180, 300
10, 14, 18	12.75	87.5	60, 180, 300
19, 20, 21	19.13	50	0, 120, 240

[a]Relative to the baffle plate which supports the bed.

[b]% of cross-sectional area.

[c]0^{o} is at the top of the sectional circles in Figure 2.

Table 2

ESEERCO TEST-BED PARTICLE SIZE DISTRIBUTION[a]

U.S. Std. Sieve Size	Percent of Total	Weight of Alloy	
		Grams	Pounds
- 4 + 10	66.83	25,460	56.14
- 10 + 16	15.18	5,784	12.75
- 16 + 20	6.14	2,339	5.16
- 20 + 25	2.23	850	1.87
- 25 + 30	2.44	930	2.05
- 30 + 35	1.70	648	1.43
- 35 + 60	4.50	1,715	3.78
- 60 + 80	0.774	295	0.65
- 80 + 100	0.203	77	0.17
- 4 + 100	100	38,100	84.0

[a]For batch NL-2 of FeTi alloy.

Table 3

ANALYSIS OF BATCH NL-2 OF FeTi ALLOY[a]

Gravimetric[a]		Spectrographic	
Element	Wt %	Element	Wt %
Fe	53.8	Ni	∿0.1
Ti	46.0	Cr	∿0.05
O	0.062	Mg	<0.001
N	0.0082		
C	0.025		

[a]As analyzed by International Nickel Co.

Table 4

SUMMARY OF ESEERCO TEST-BED DATA FOR SUSTAINED-FLOW-RATE RUNS[a]

ESEERCO	Constant-Flow-Rate-Period					Variable-Flow-Rate-Period				Totals	
Run No.	P_1 PSIA	Rate SLPM	Time Min	Wt Lb	P_2 PSIA	Time Min	Wt Lb	P_3 PSIA	Rate SLPM	Wt Lb	Time Min
E03C1	71.7	40	72	C.532	496	179	0.375	501	3.83	0.907	251
E03C2	266	20	15	C.0565	493	69	0.0355	499	1.41	0.092	84
E03D1	499	40	79	C.579	26.4	169	0.454	16.2	6.60	1.033	248
E03D2	55.4	10	11	0.0200	20.9	2	0.0037	18.2	8.85	0.0237	13
E04C1	39.7	30	115	0.648	492	169	0.331	498	4.13	0.979	284
E04D1	492	30	115	0.635	28.8	133	0.332	16.9	6.80	0.968	248
E04D2	51.5	10	12	0.0214	18.4	2	0.0031	17.1	6.88	0.0246	14
E05C1	37.3	25	152	0.751	494	153	0.250	500	3.87	1.001	315
E05D1	504	25	154	0.712	26.1	117	0.258	16.7	6.33	0.970	271
E05D2	57.6	5	33	0.0309	18.3	0	0	--	--	0.0309	33
E06C1	28.5	20	224	0.832	498	116	0.168	501	3.81	1.000	340
E06D1	503	20	214	0.796	23.1	127	0.204	16.0	4.13	1.000	341
E07C1	32.0	15	324	0.903	499	84	0.097	500	3.49	1.000	408
E07D1	511	15	315	0.878	20.3	87	0.122	15.8	3.72	1.000	402
E08C1	30.2	10	529	C.967	498	36	0.033	498	3.61	1.000	555
E08D1	502	10	510	C.951	18.0	55	0.049	15.6	2.73	1.000	565

[a]For batch NL-2 of FeTi alloy. H_2O conditions: 2 GPM, 30°C (86°F) for charging, 50°C (122°F) for discharging. In the Run No., C = Charging and D = Discharging.

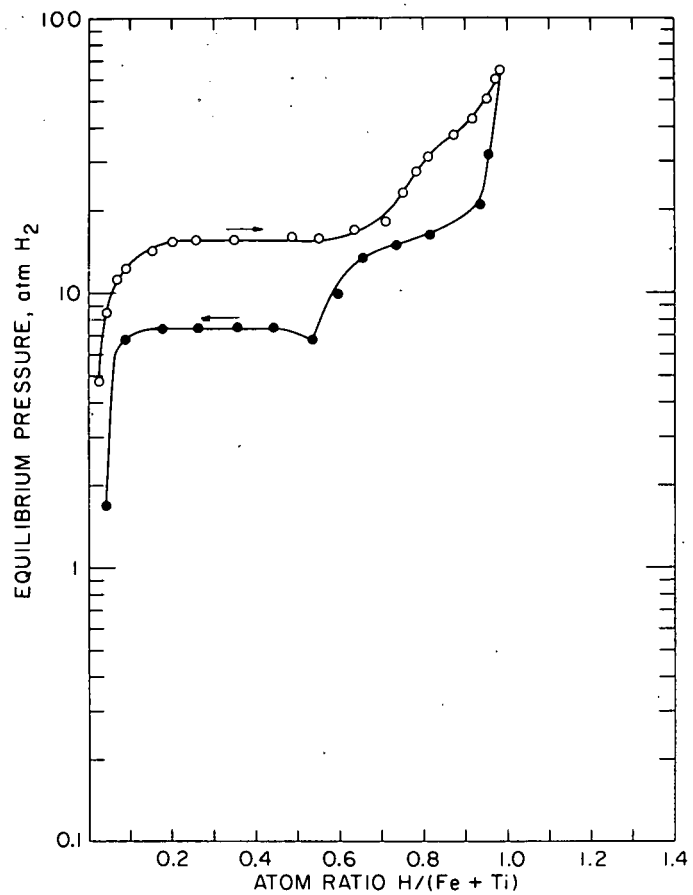

Figure 1. Pressure-composition relationships for the FeTi-H system at 40°C (104°F).

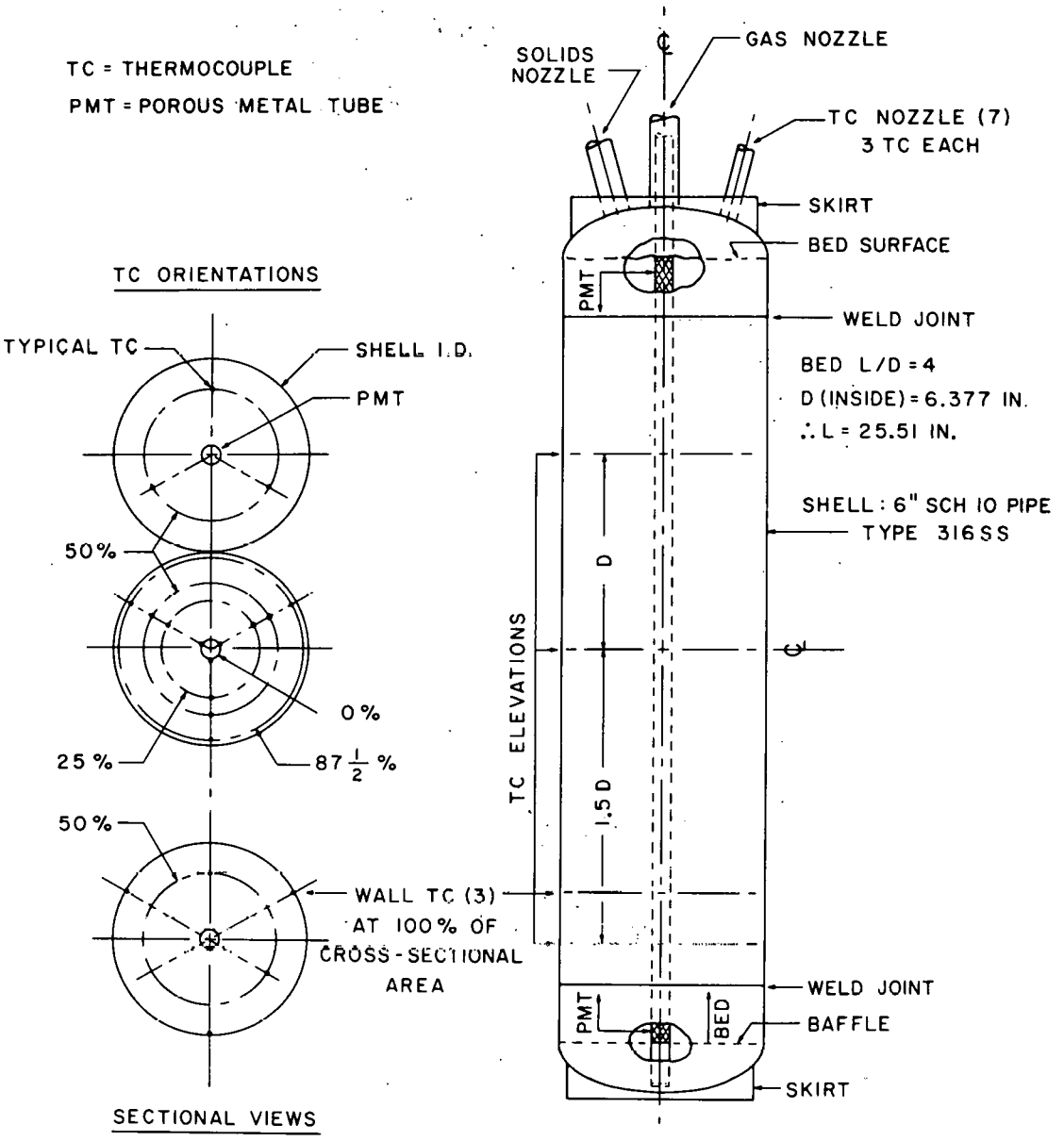

Figure 2. Sketch of ESEERCO Test Bed.

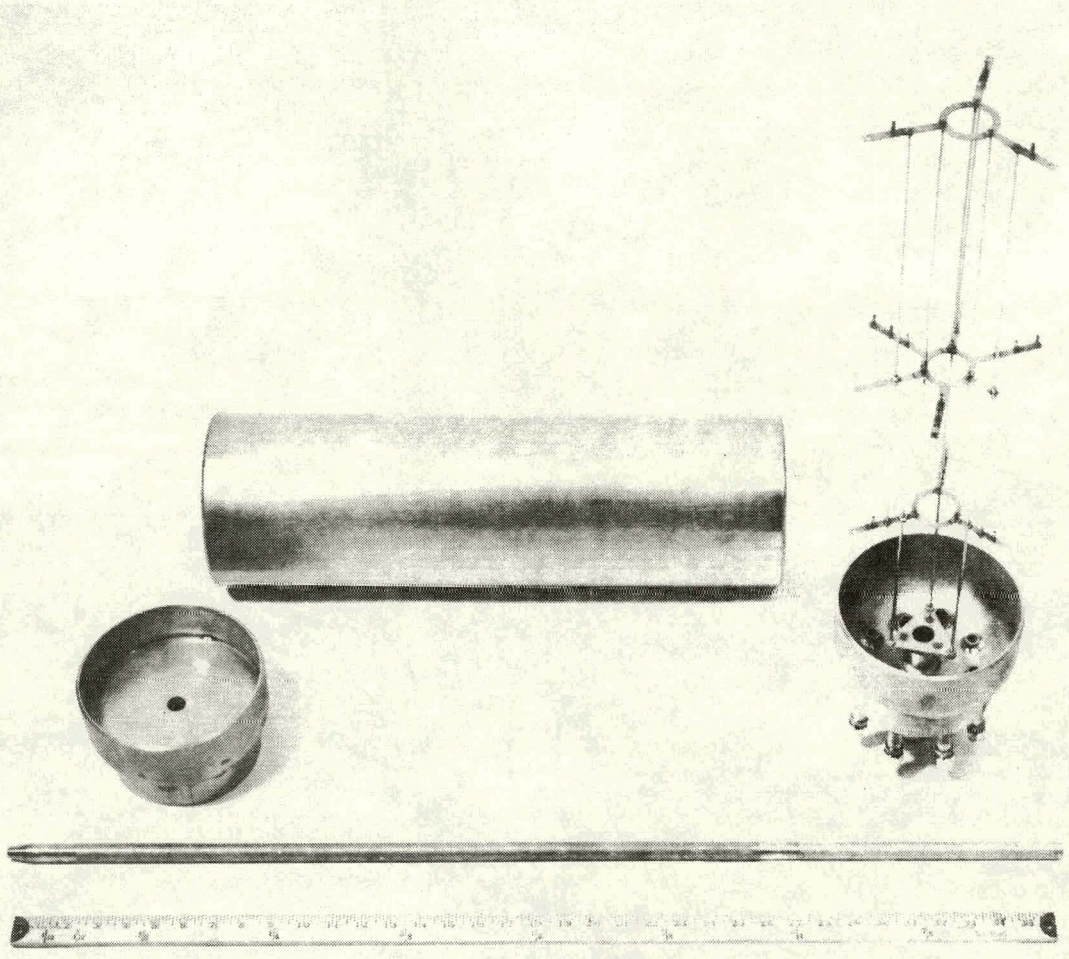

Figure 3. Major components of ESEERCO Test Bed.

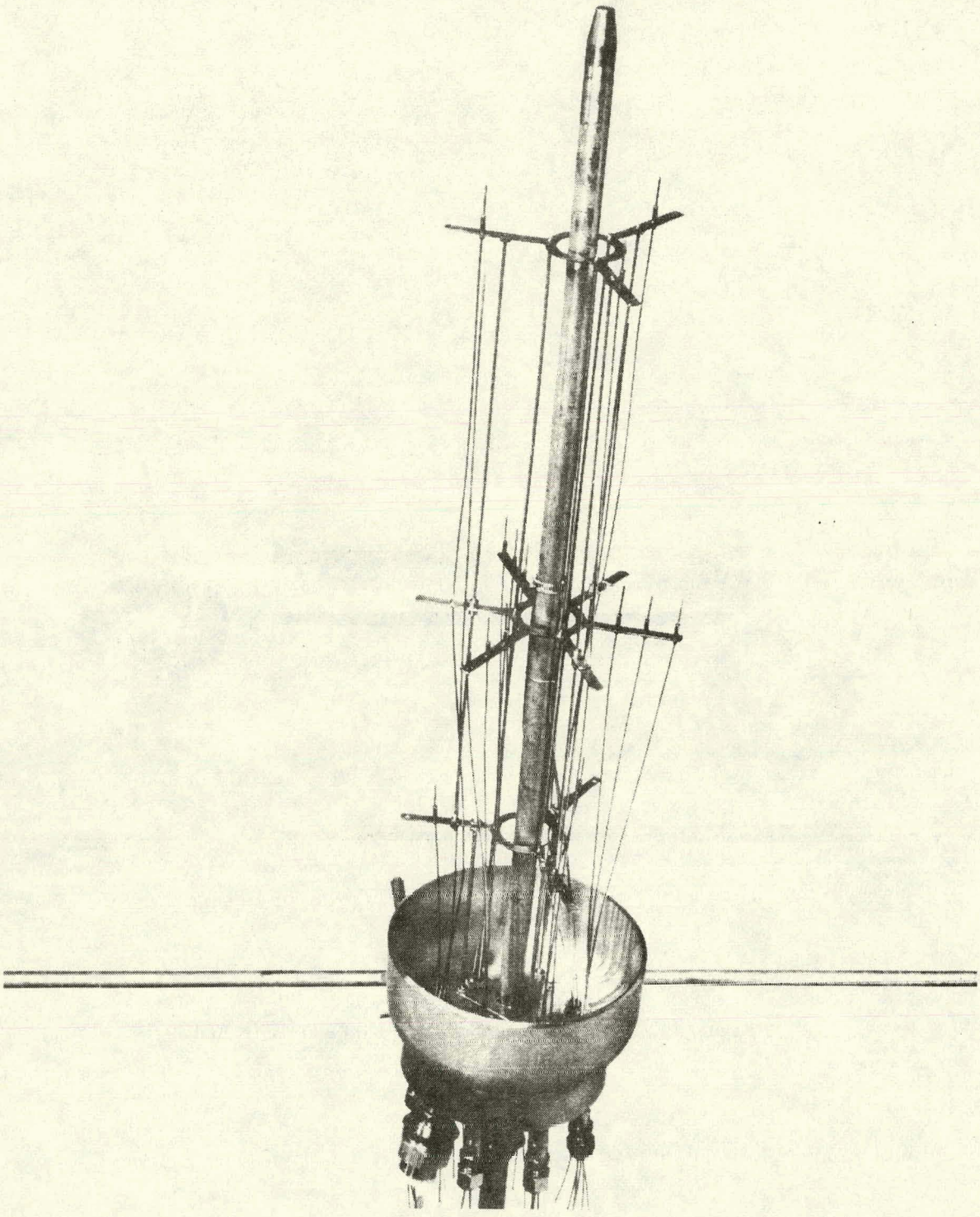

Figure 4. Upper cap assembly of ESEERCO Test Bed with thermocouples and porous metal tube.

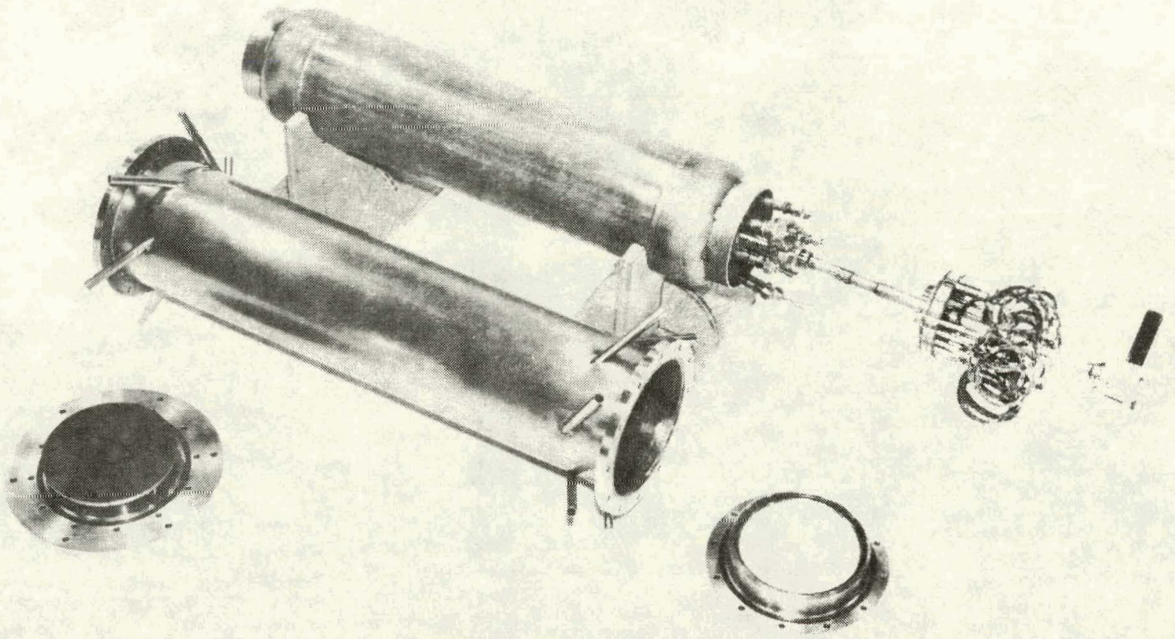

Figure 5. Completed vessel and removable water jacket for ESEERCO Test Bed.

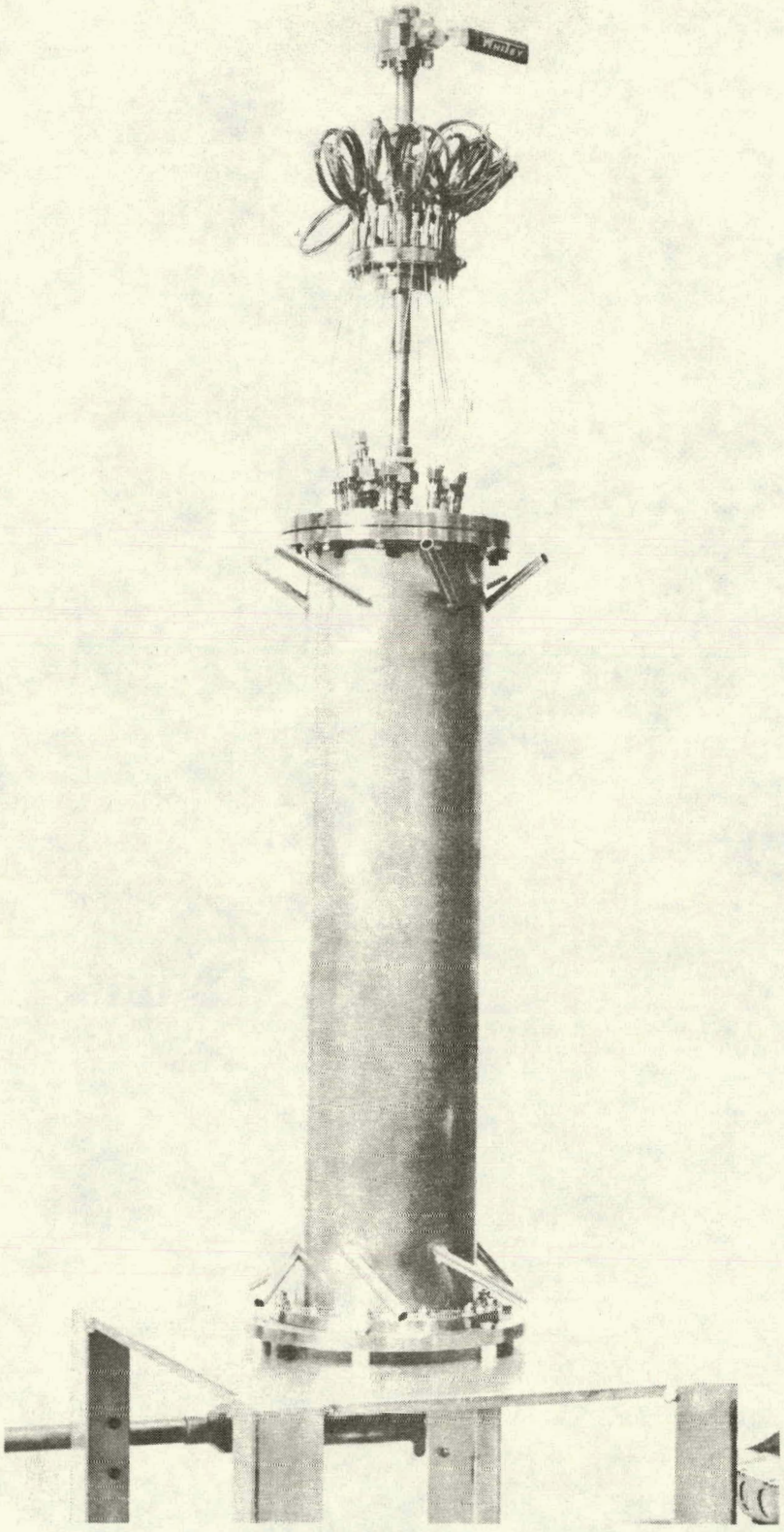

Figure 6. Assembled ESEERCO Test Bed mounted on its operating stand.

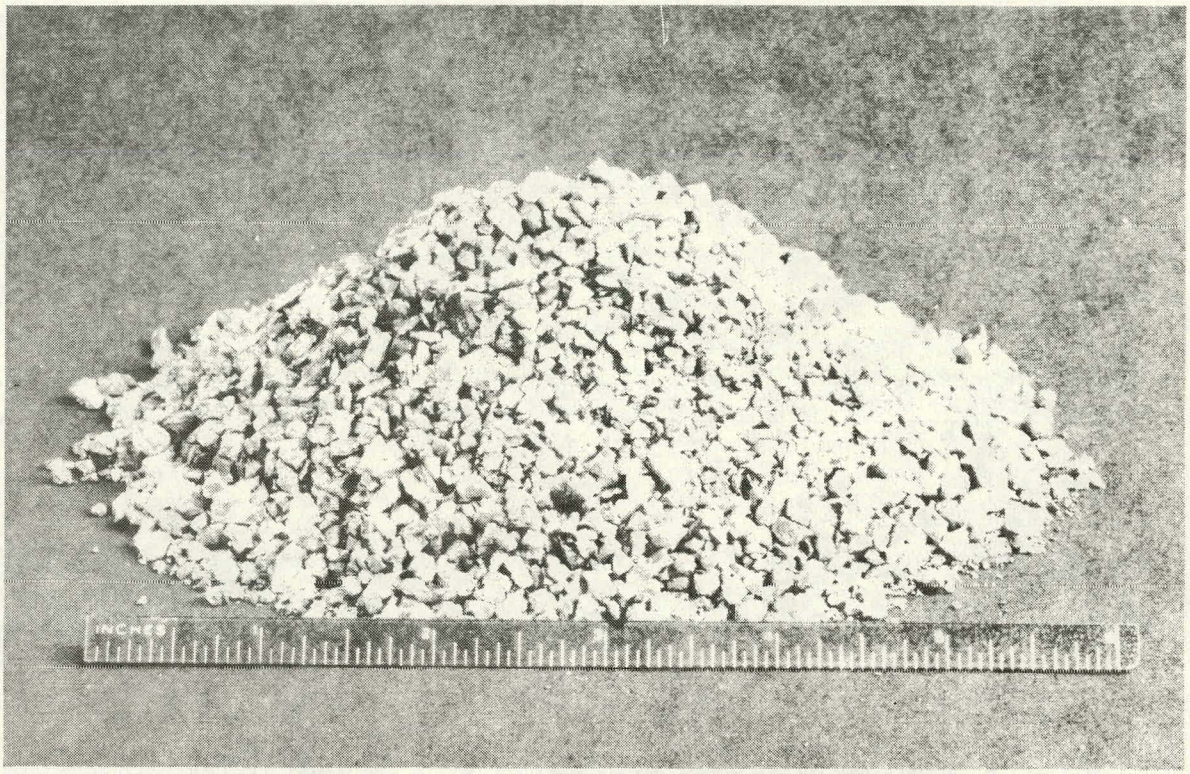

Figure 7. Full-scale picture of FeTi alloy, -4 + 100 mesh size.

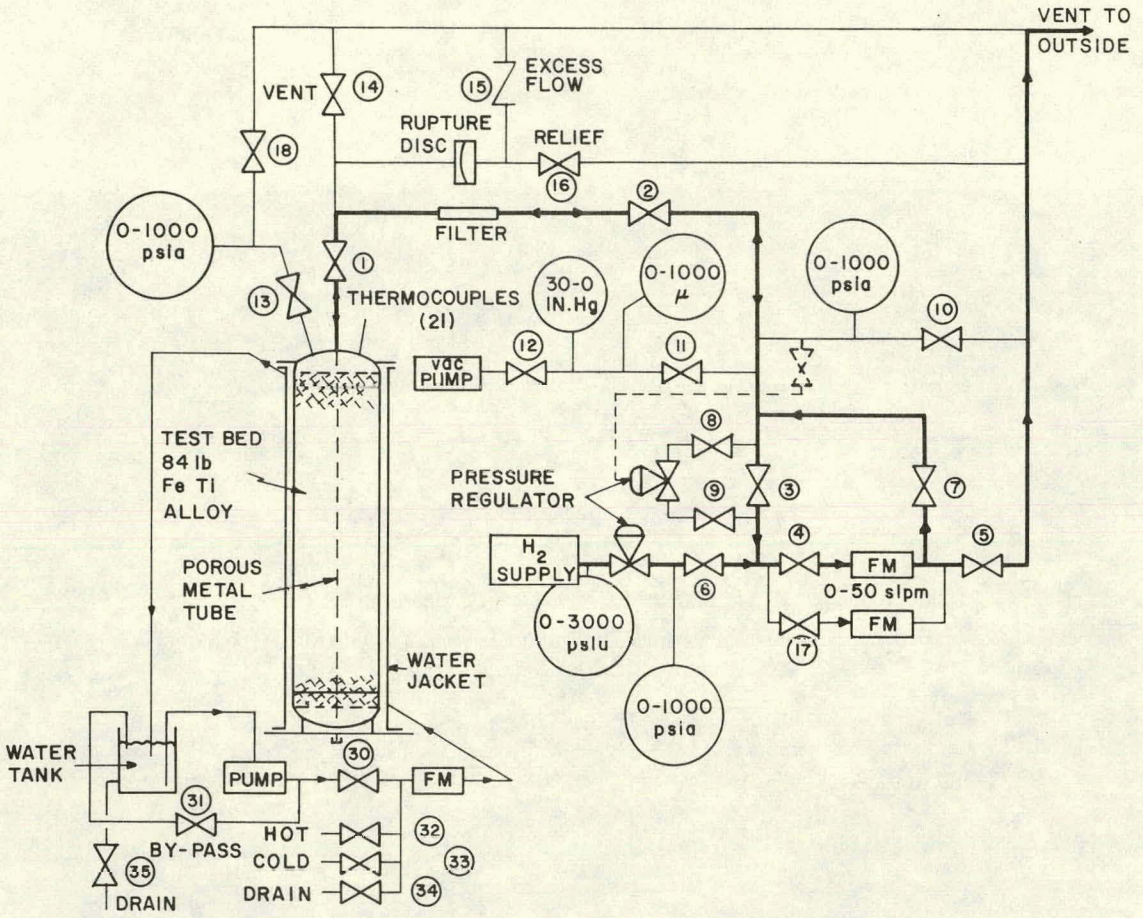

Figure 8. Equipment flow diagram for the ESEERCO Test Bed.

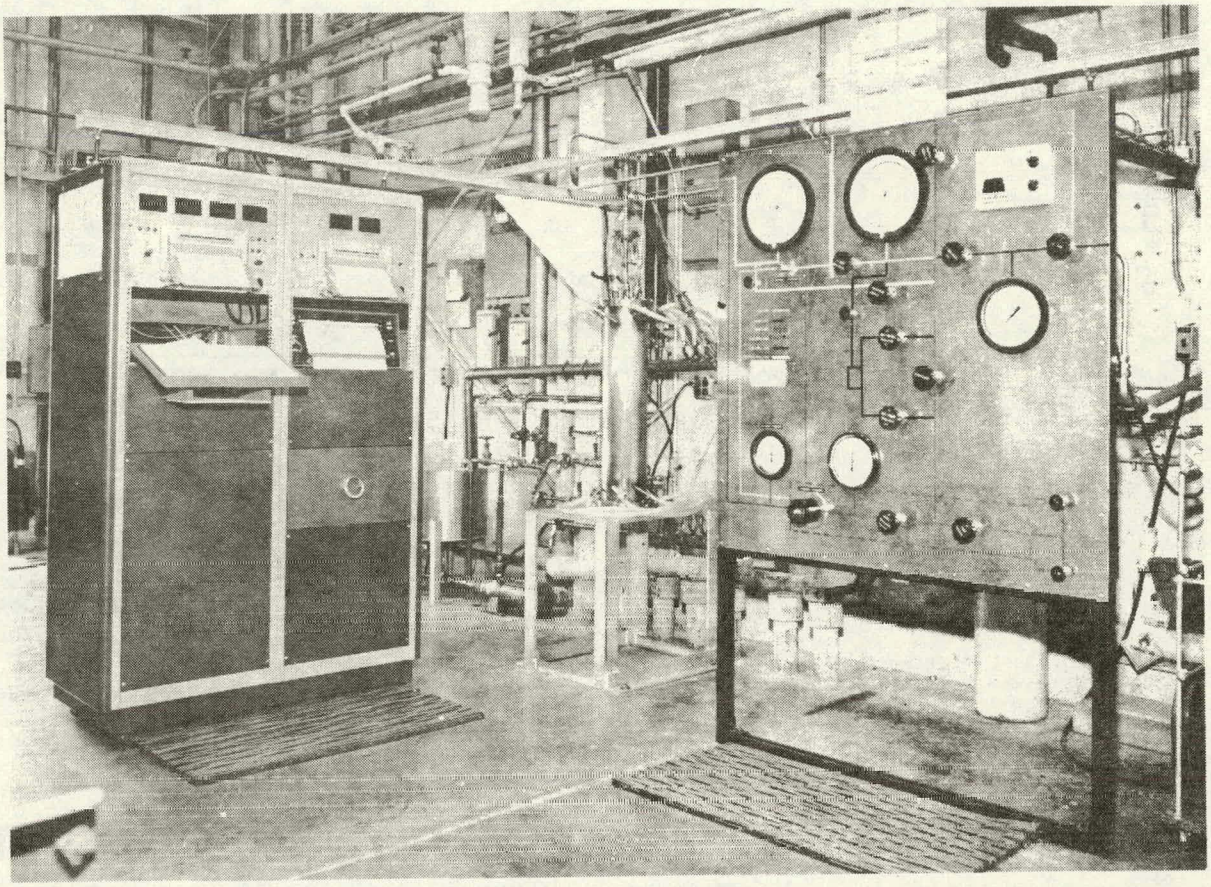

Figure 9. View of the ESEERCO Test Bed operating area.

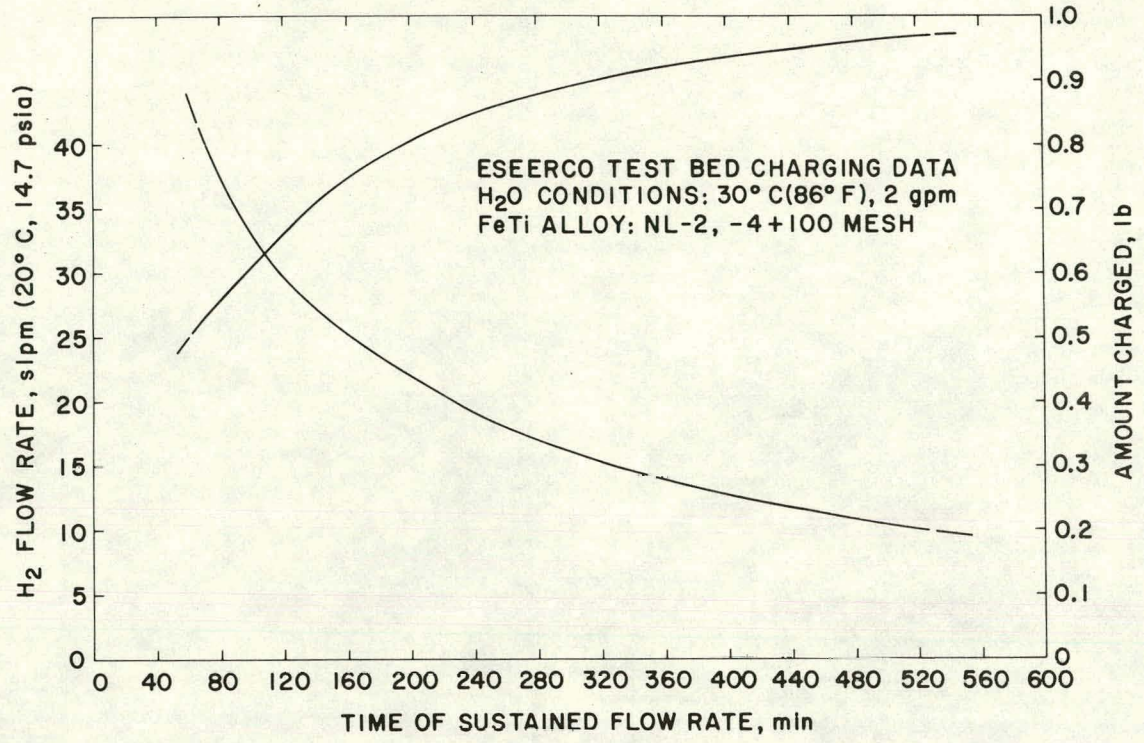

Figure 10. ESEERCO Test Bed performance during hydriding.

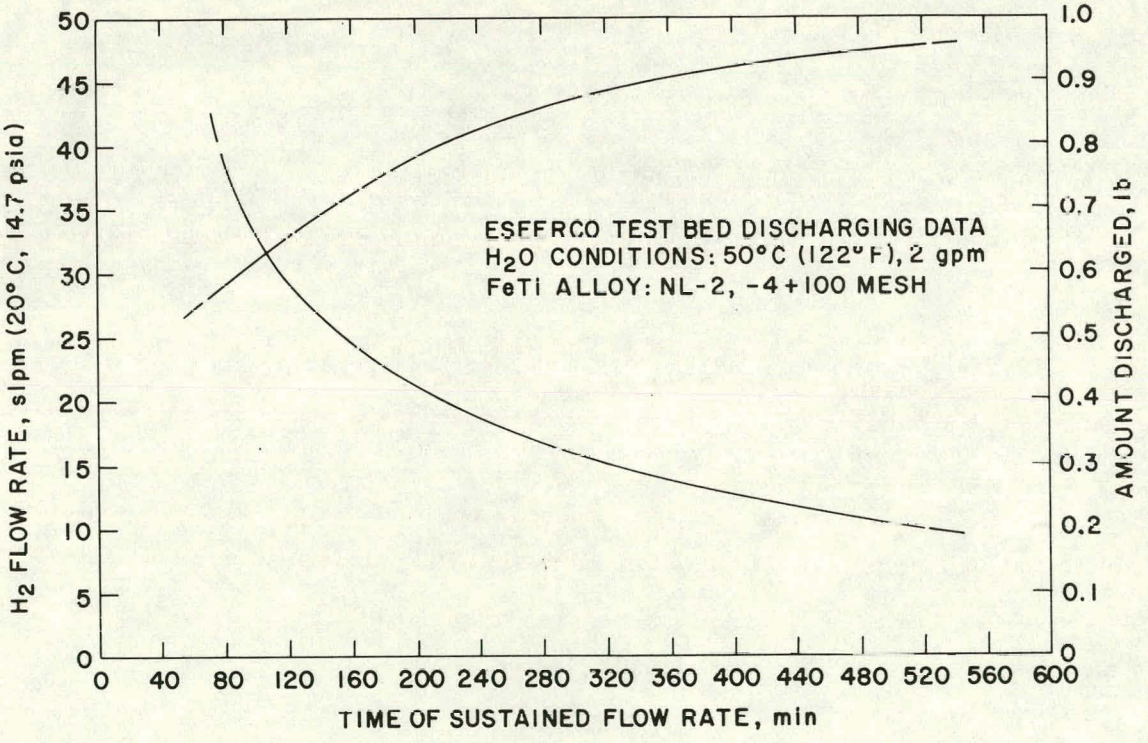

Figure 11. ESEERCO Test Bed performance during dehydriding.

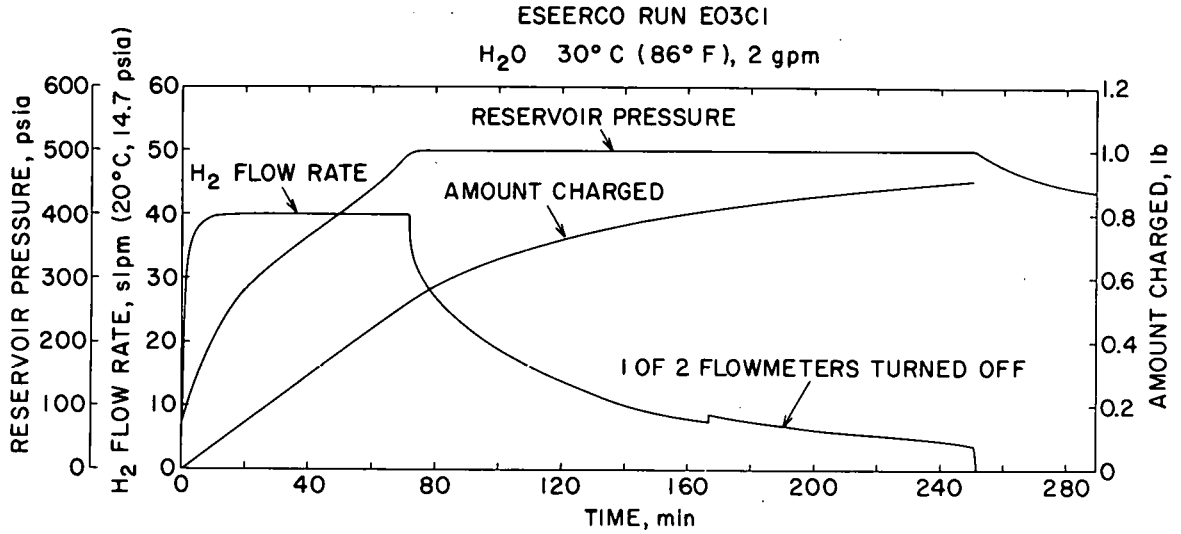

Figure 12. Reservoir pressure, hydrogen flow rate and amount charged during Run E03C1.

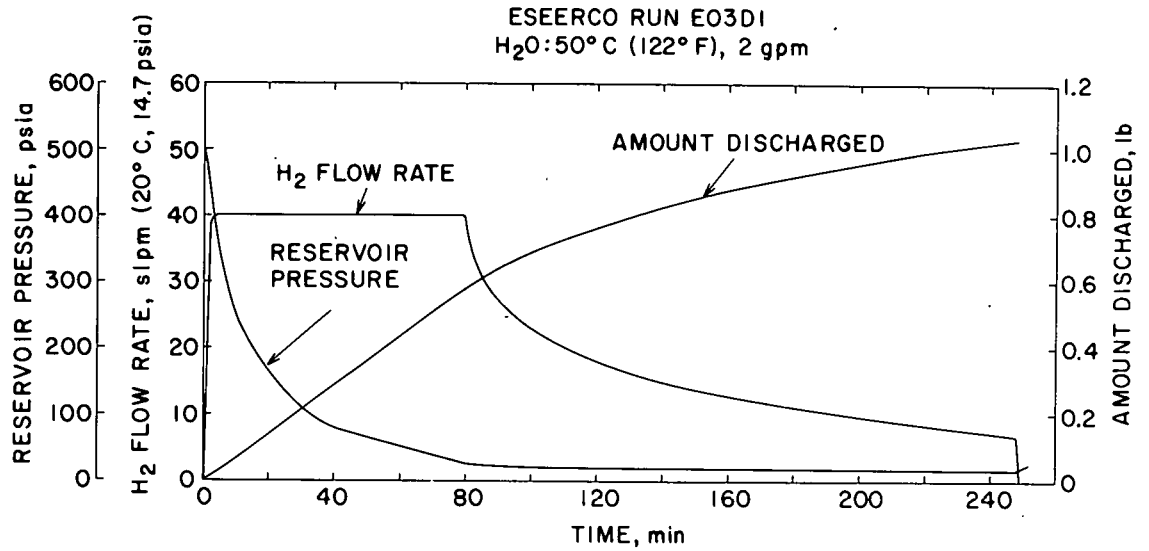

Figure 13. Reservoir pressure, hydrogen flow rate and amount discharged during Run E03D1.

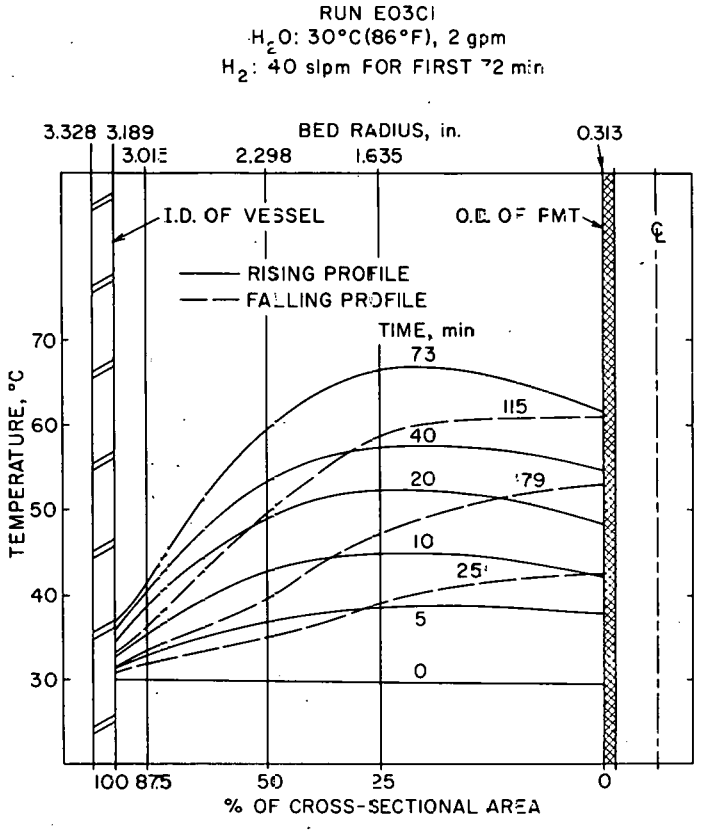

Figure 14. Temperature profiles for Run E03C1.

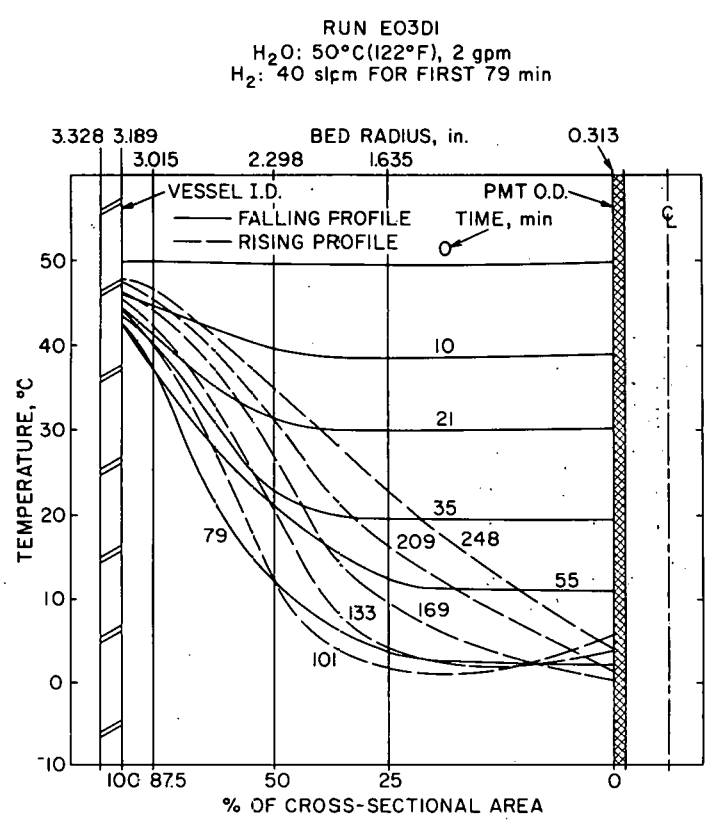

Figure 15. Temperature profiles for Run E03D1.

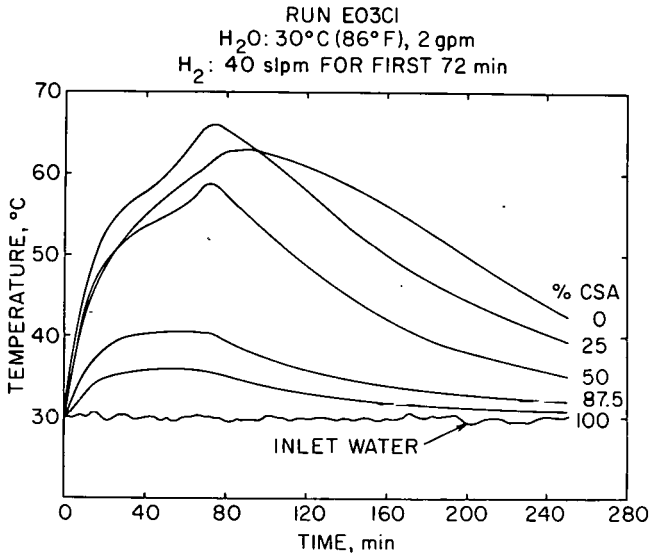

Figure 16. Temperature history for Run E03C1.

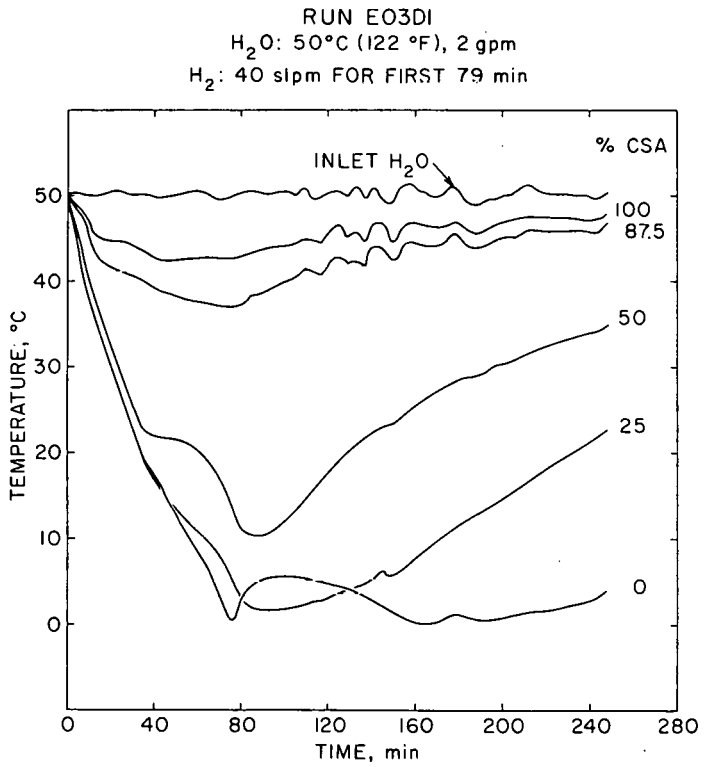

Figure 17. Temperature history for Run E03D1.

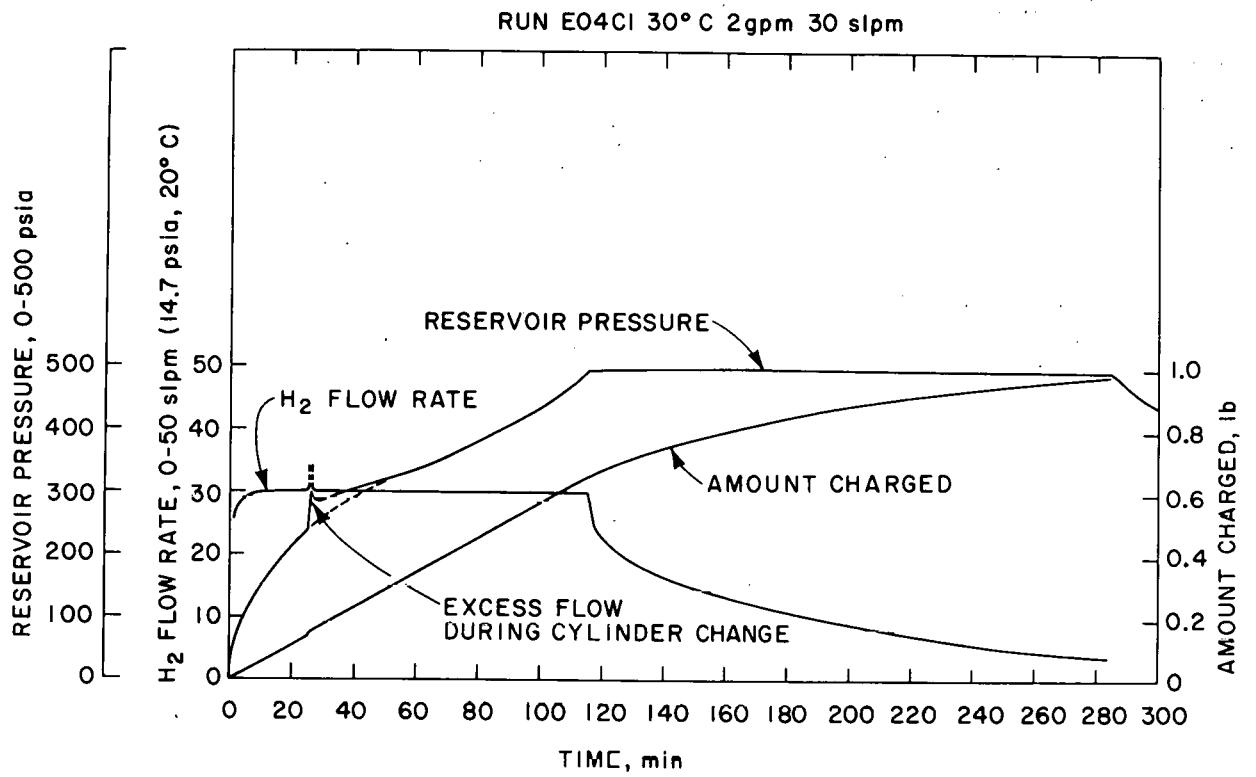

Figure 18. Reservoir pressure, hydrogen flow rate and amount charged during Run E04C1.

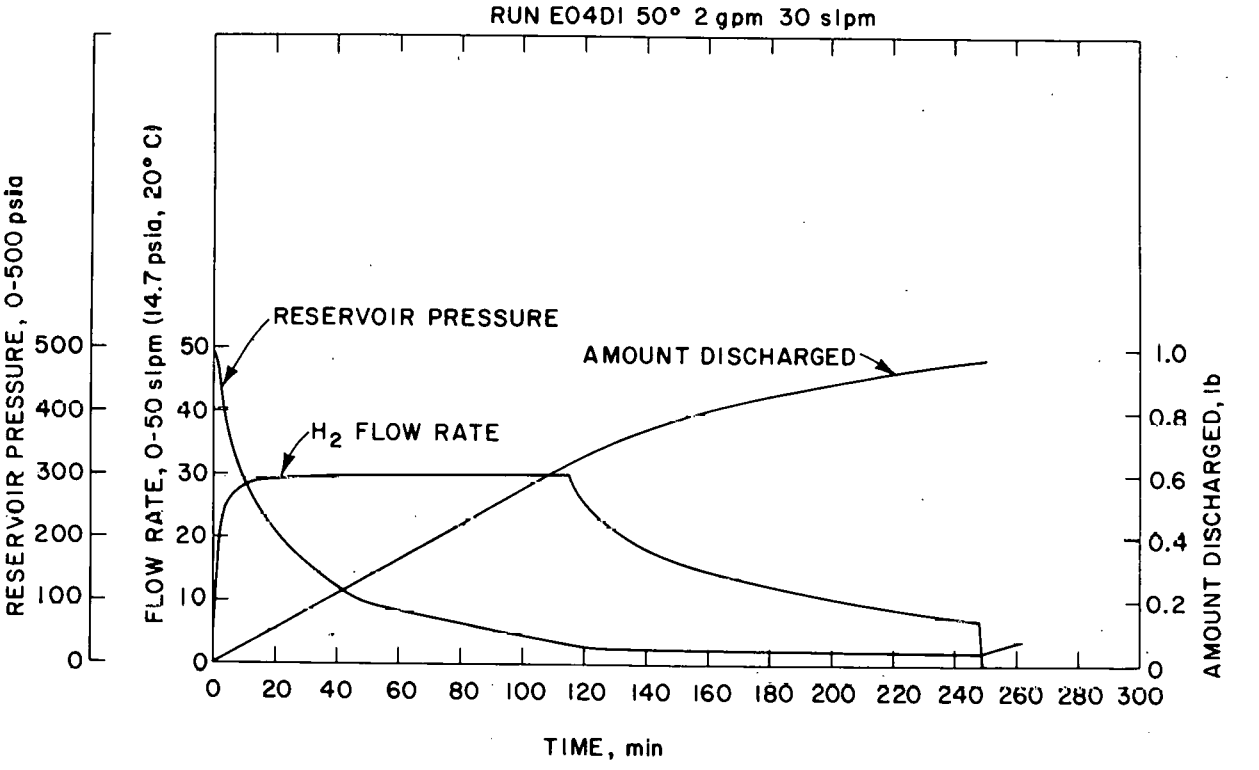

Figure 19. Reservoir pressure, hydrogen flow rate and amount discharged during Run E04D1.

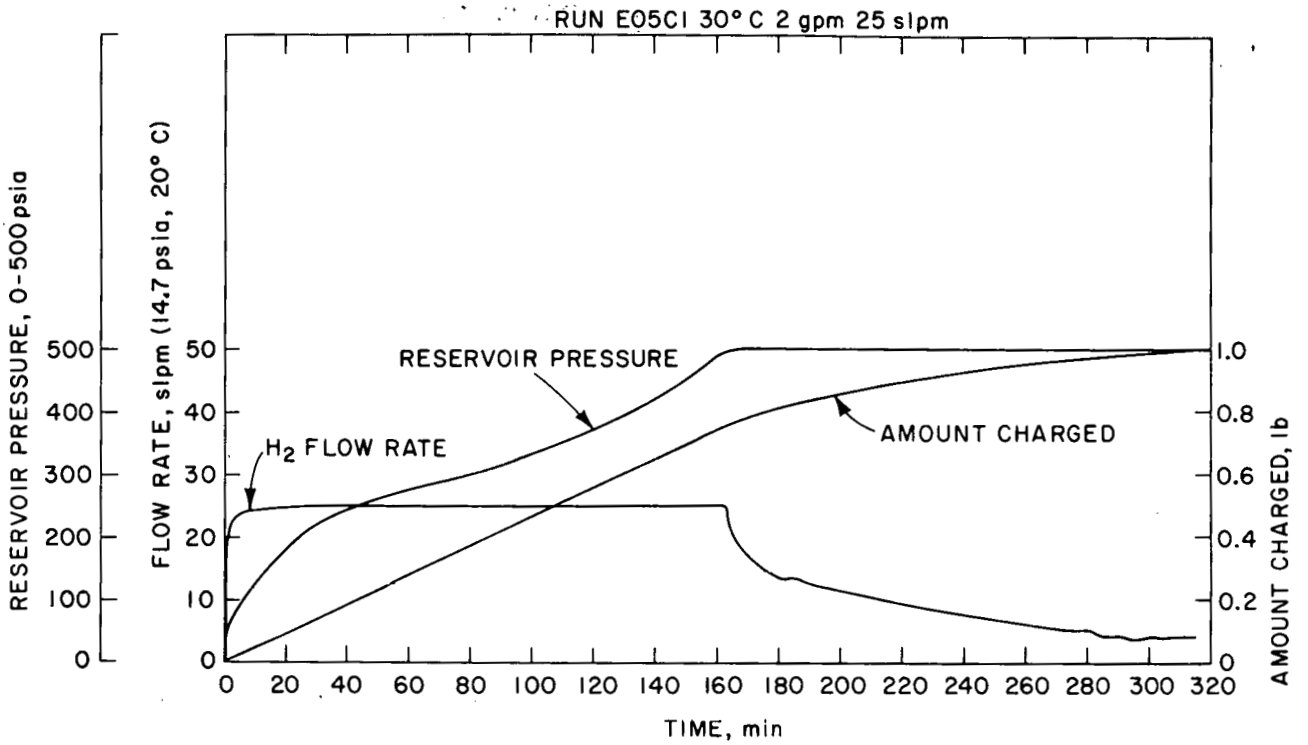

Figure 20. Reservoir pressure, hydrogen flow rate and amount charged during Run E05C1.

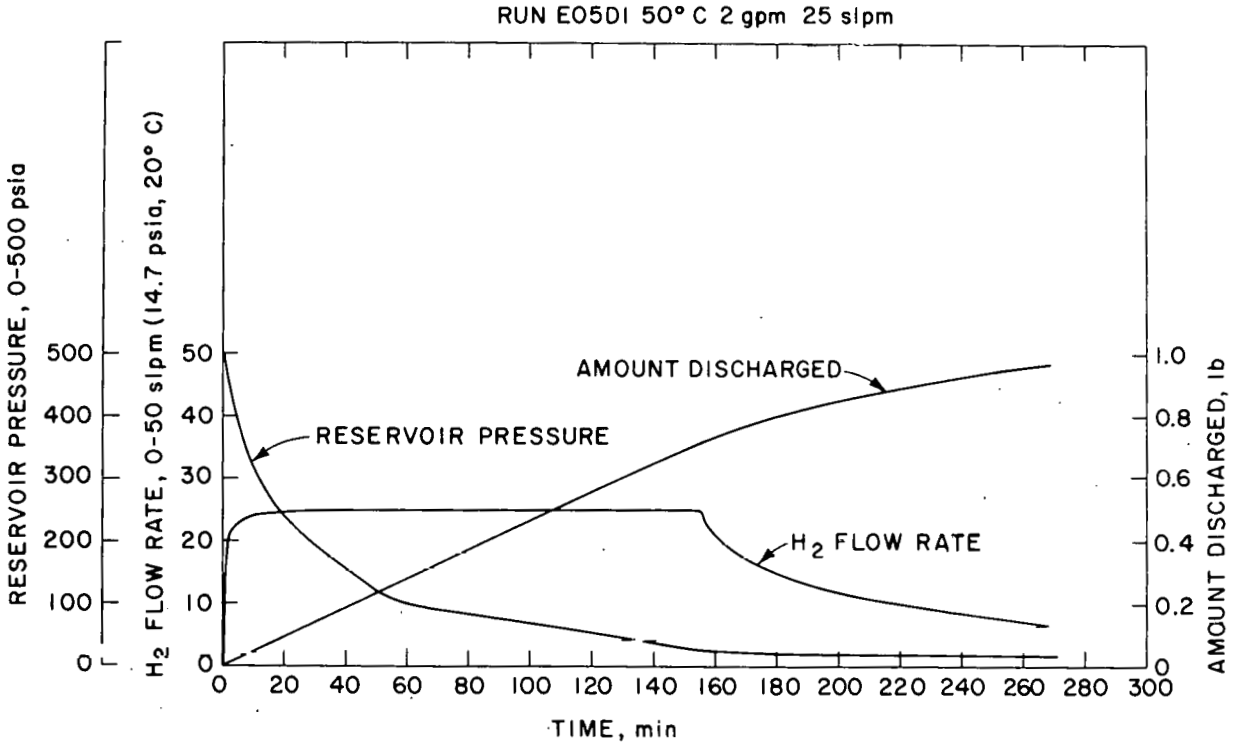

Figure 21. Reservoir pressure, hydrogen flow rate and amount discharged during Run E05D1.

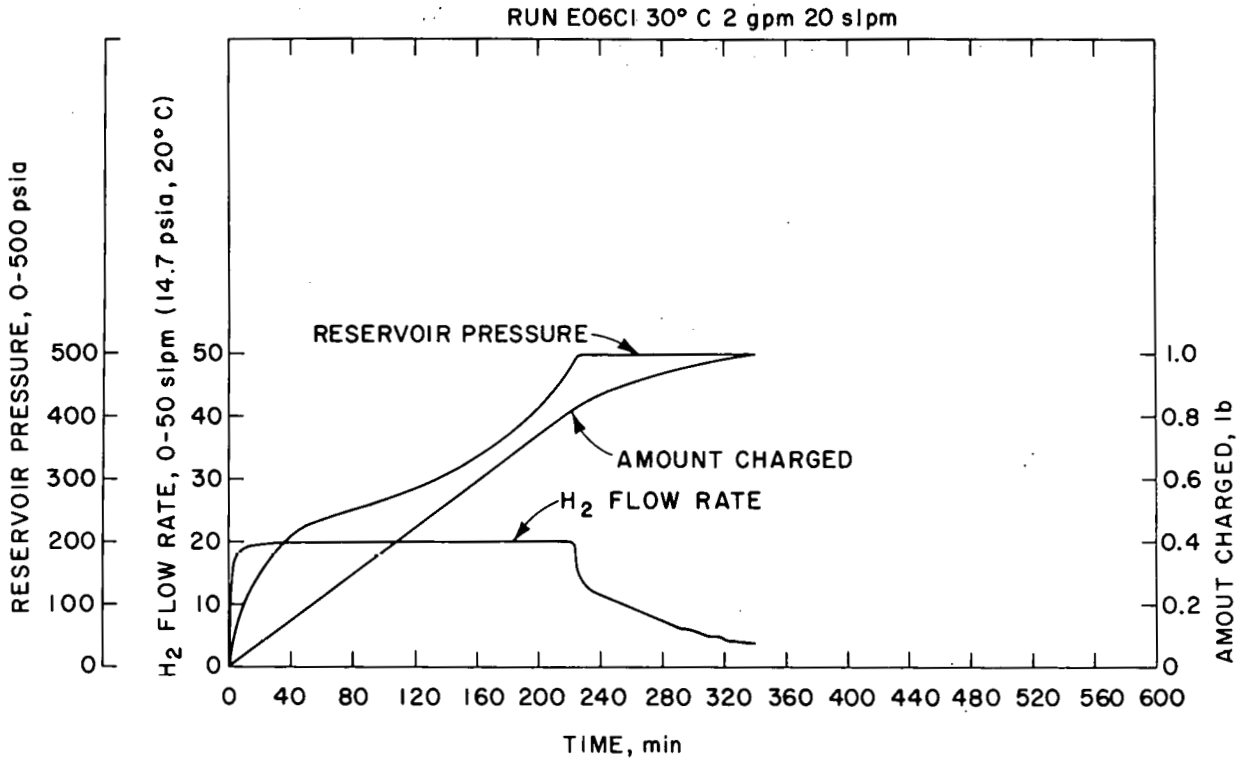

Figure 22. Reservoir pressure, hydrogen flow rate and amount charged during Run E06C1.

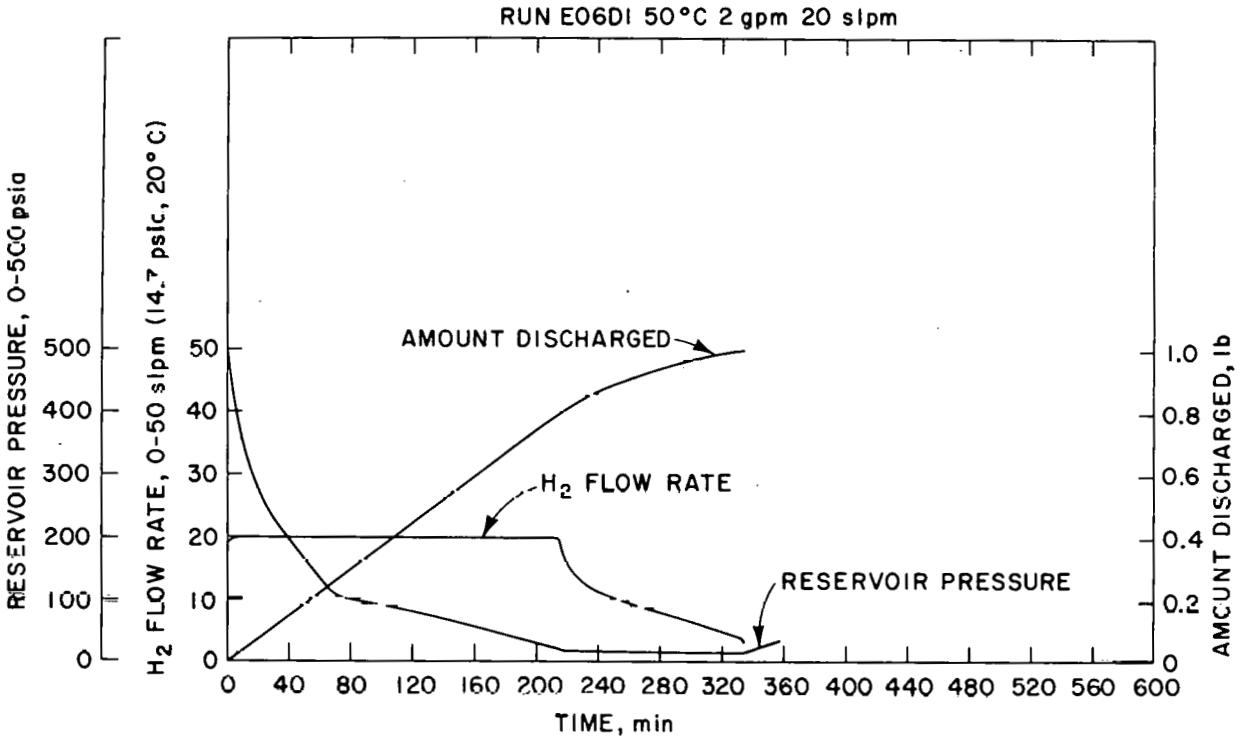

Figure 23. Reservoir pressure, hydrogen flow rate and amount discharged during Run E06D1.

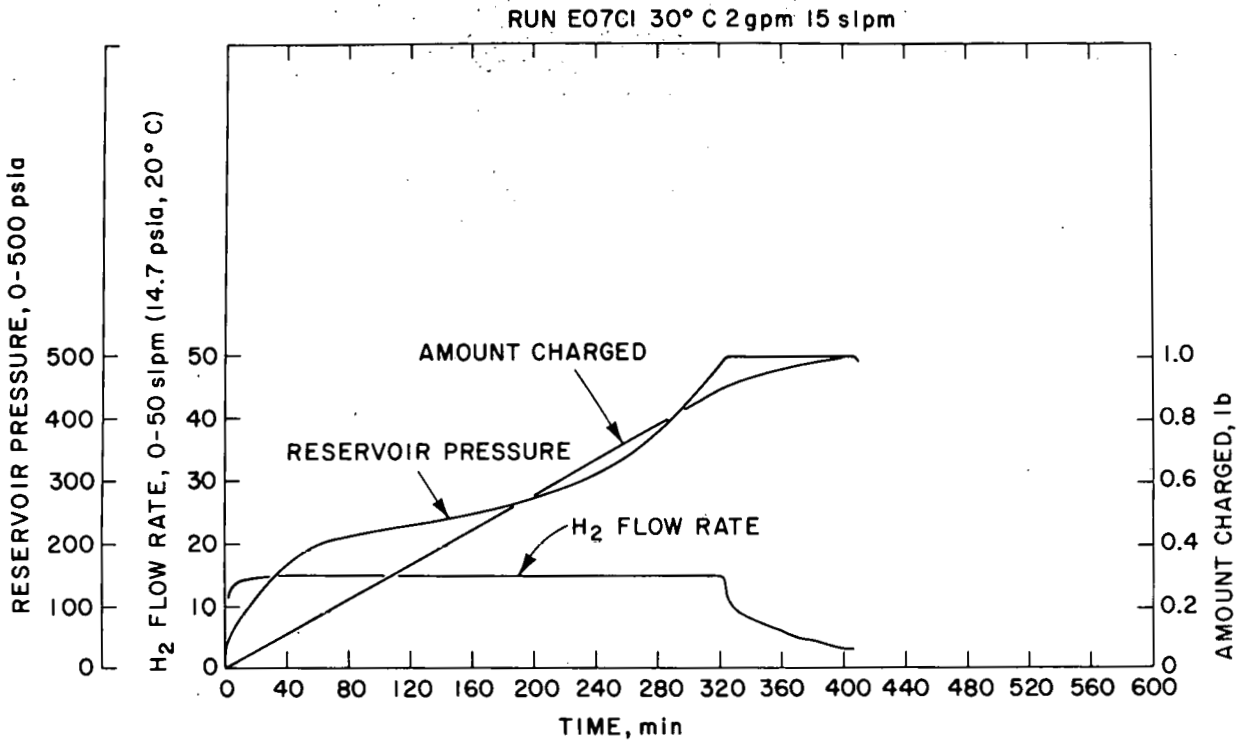

Figure 24. Reservoir pressure, hydrogen flow rate and amount charged during Run E07C1.

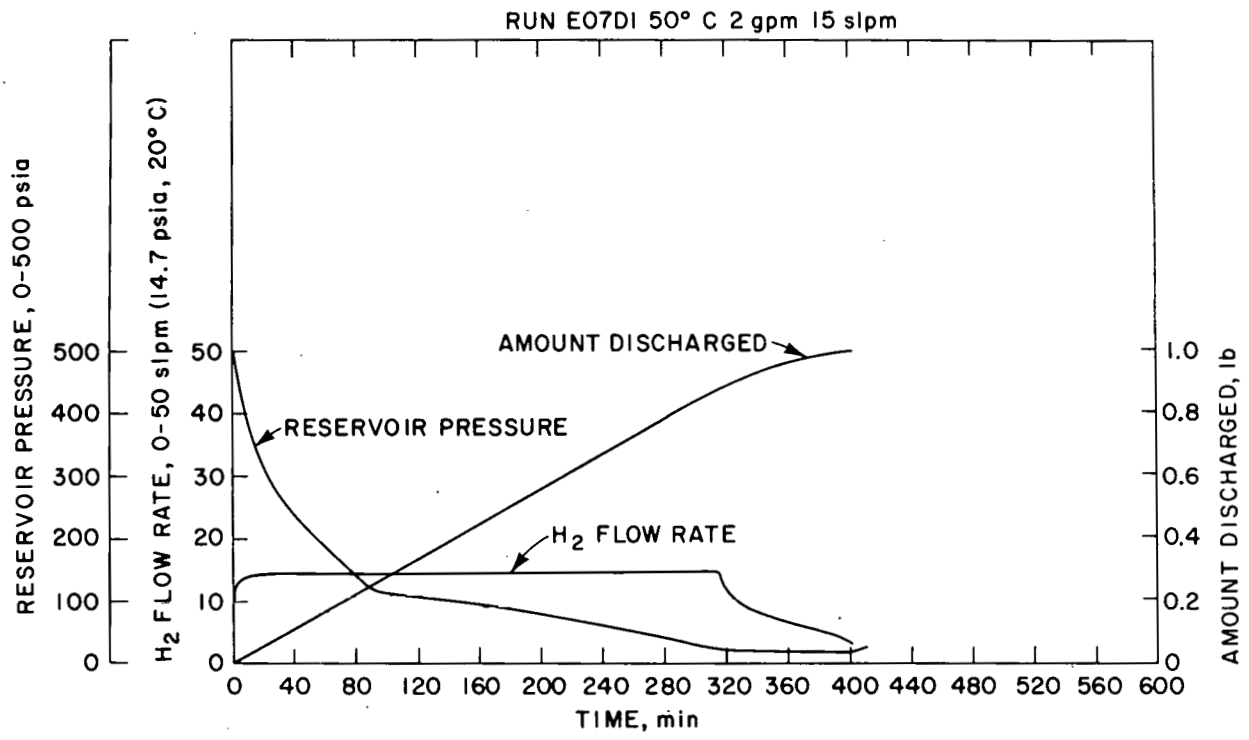

Figure 25. Reservoir pressure, hydrogen flow rate and amount discharged during Run E07D1.

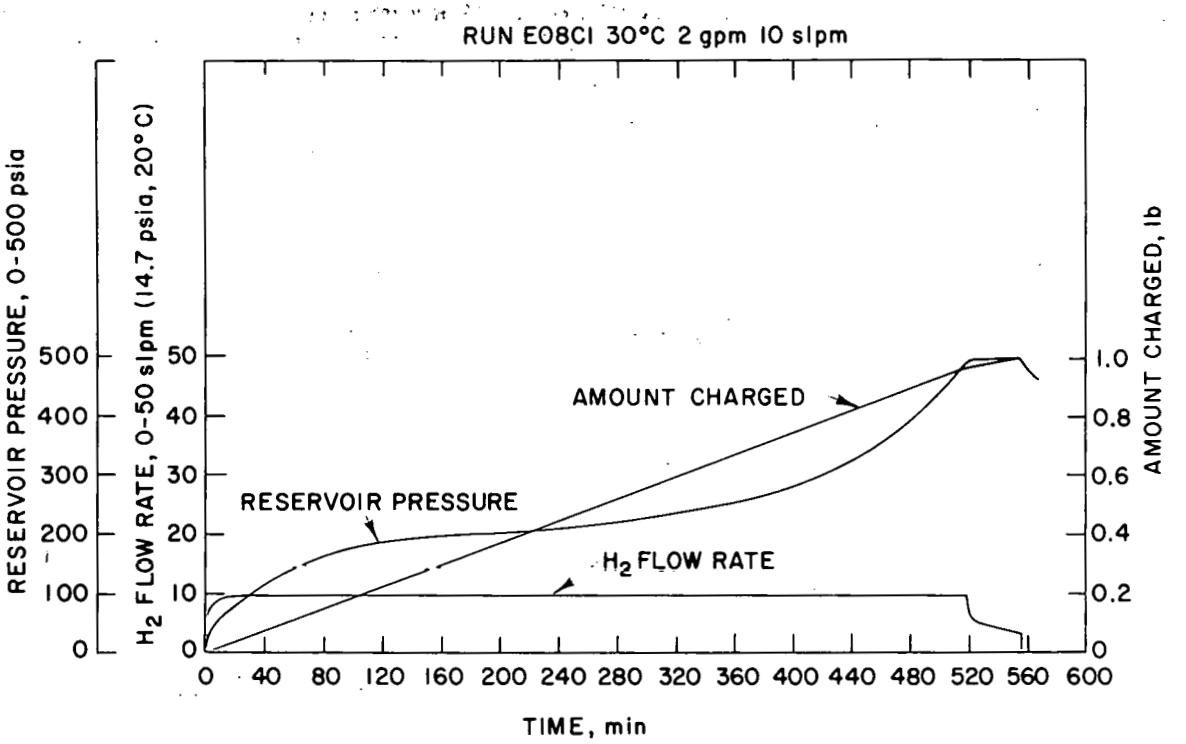

Figure 26. Reservoir pressure, hydrogen flow rate and amount charged during Run E08C1.

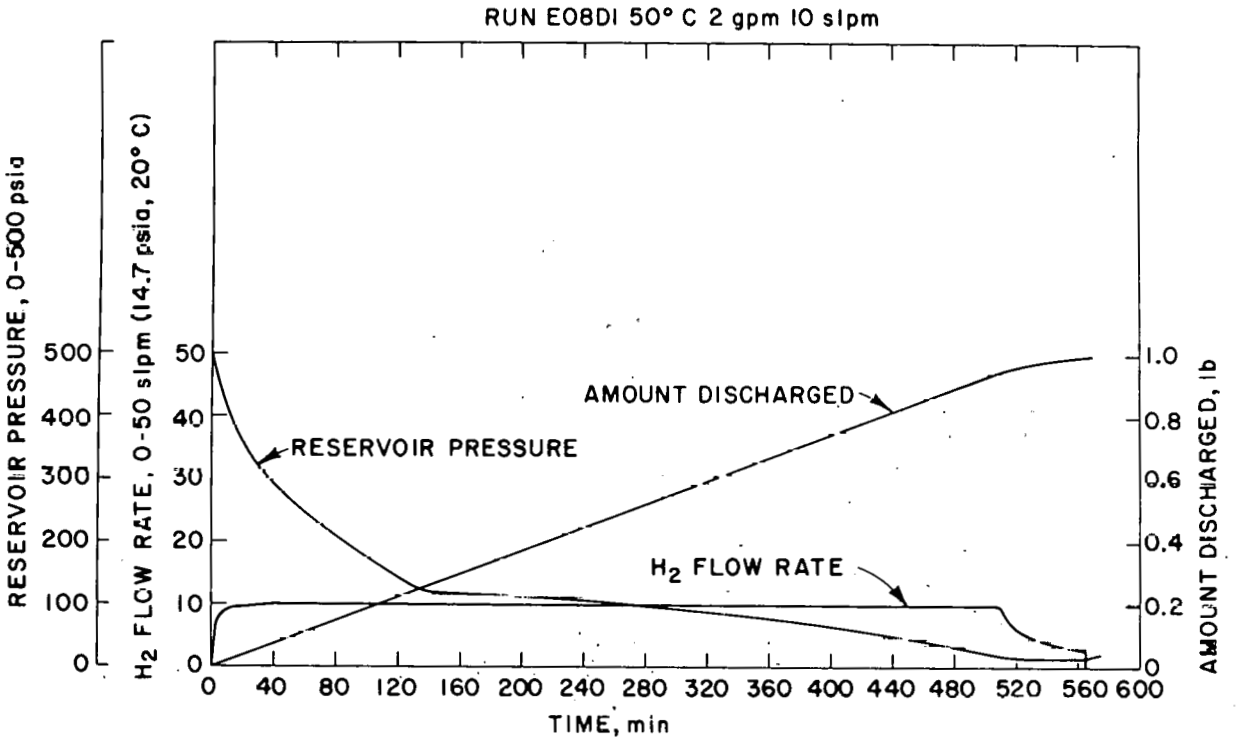

Figure 27. Reservoir pressure, hydrogen flow rate and amount discharged during Run E08D1.

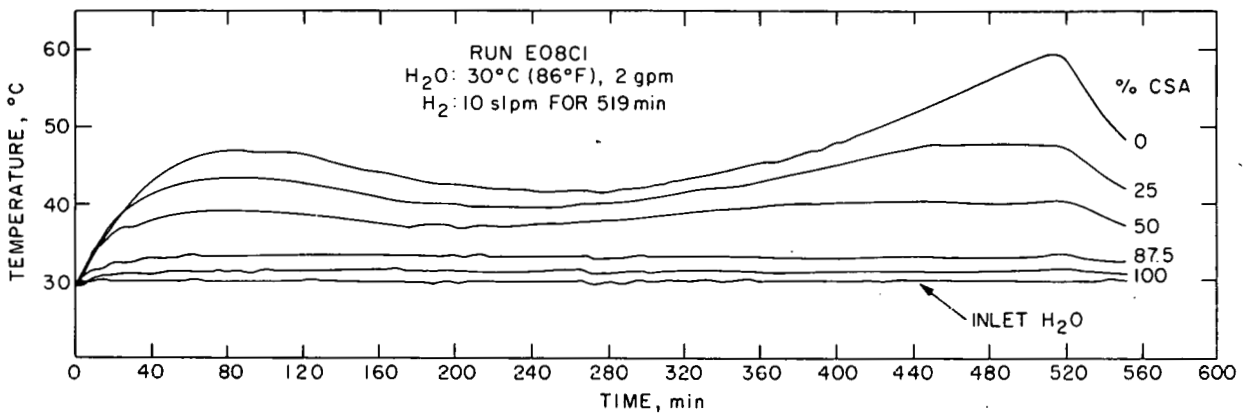

Figure 28. Temperature history for Run E08C1.

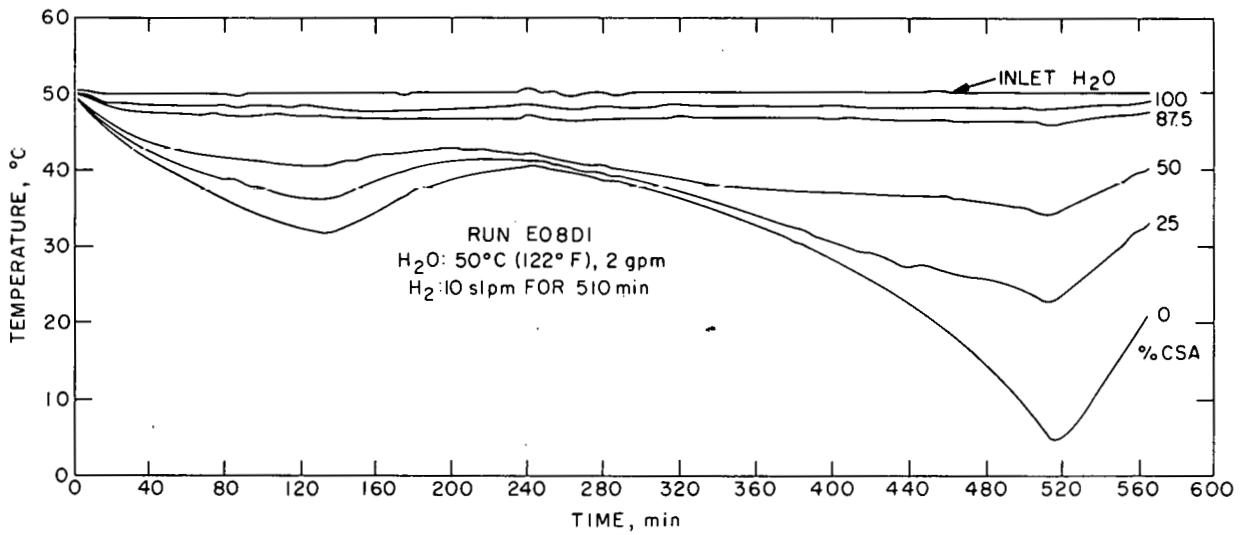

Figure 29. Temperature history for Run E08D1.

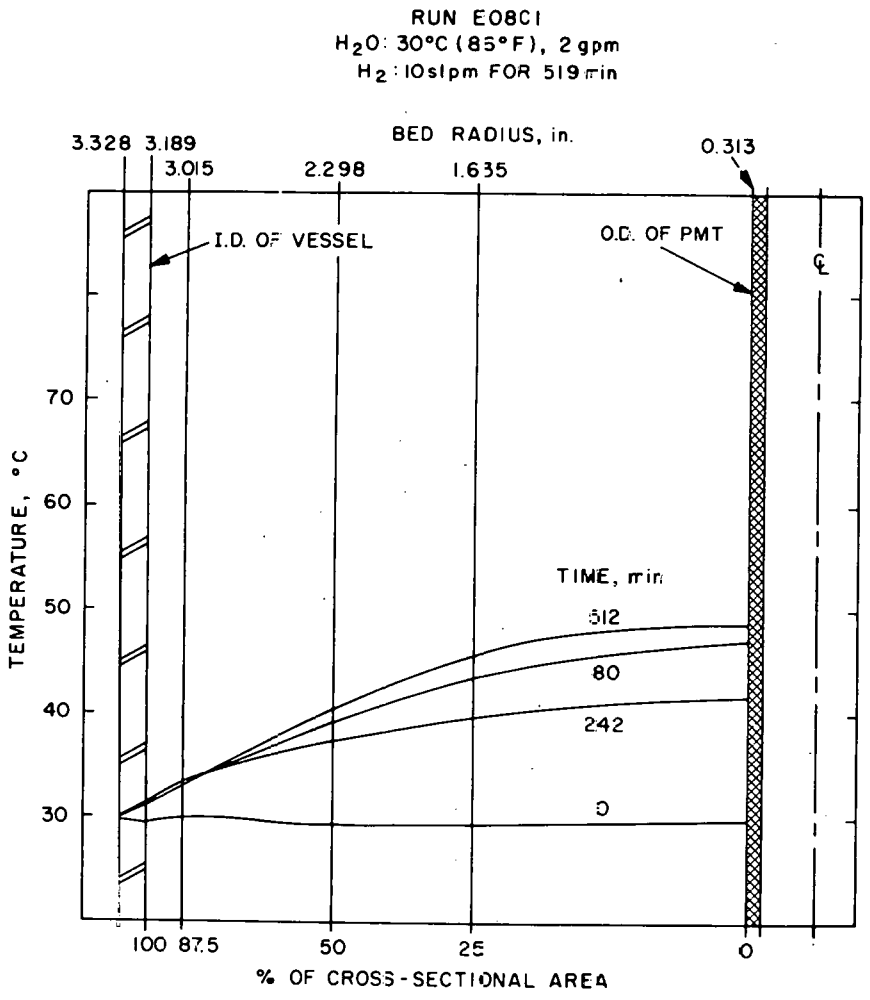

Figure 30. Temperature profiles for Run E08C1.

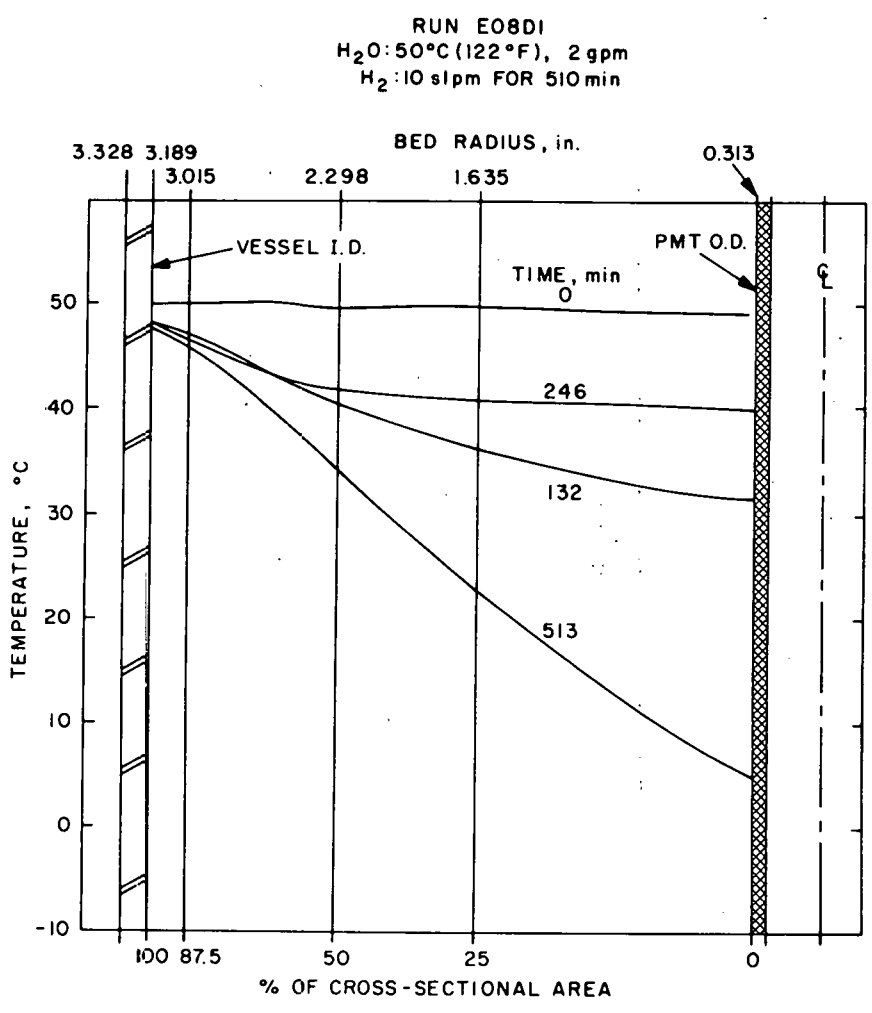

Figure 31. Temperature profiles for Run E08D1.

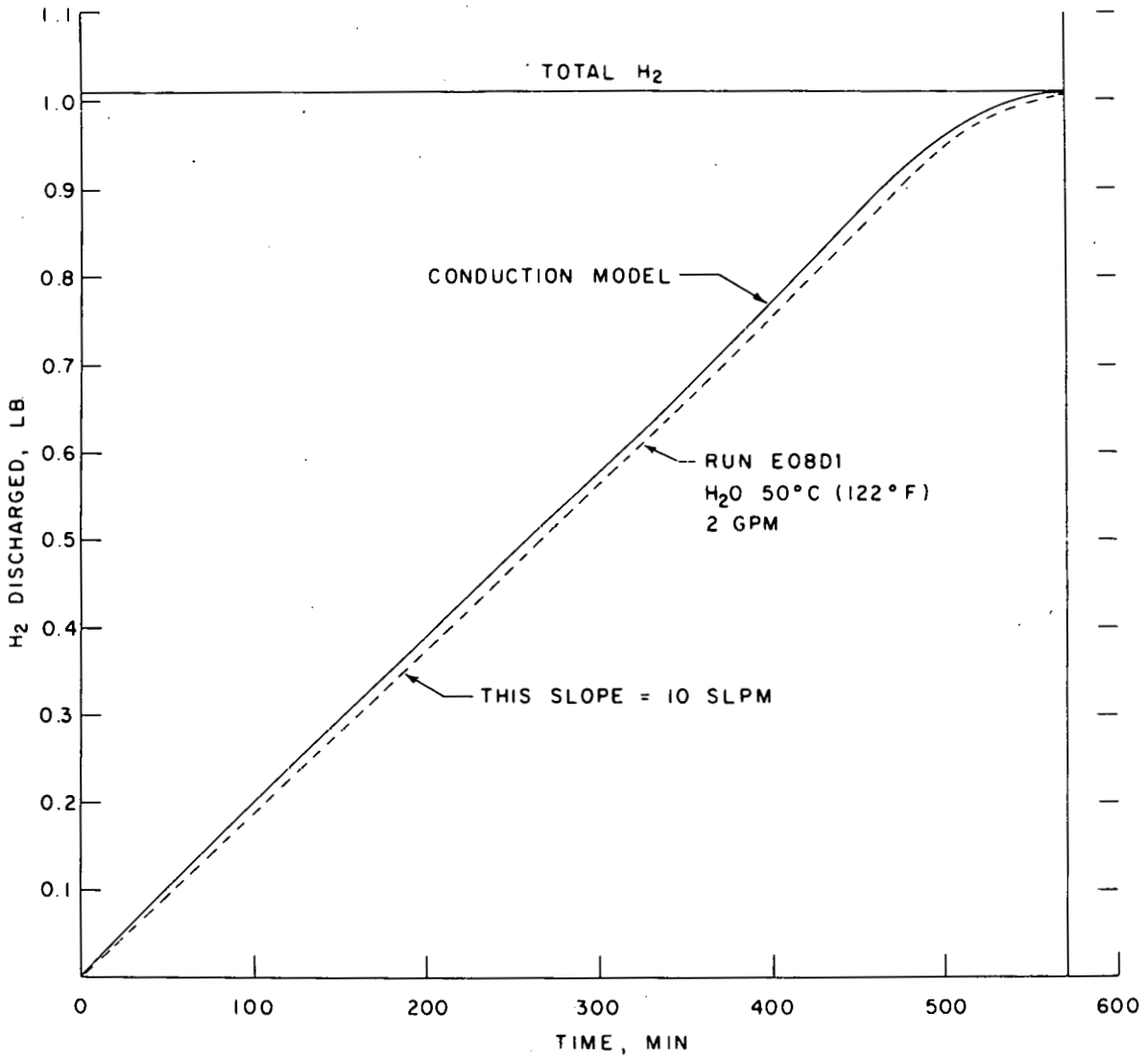

Figure 32. Comparison of experimental and analytical results for amount of hydrogen discharged during Run E08D1.

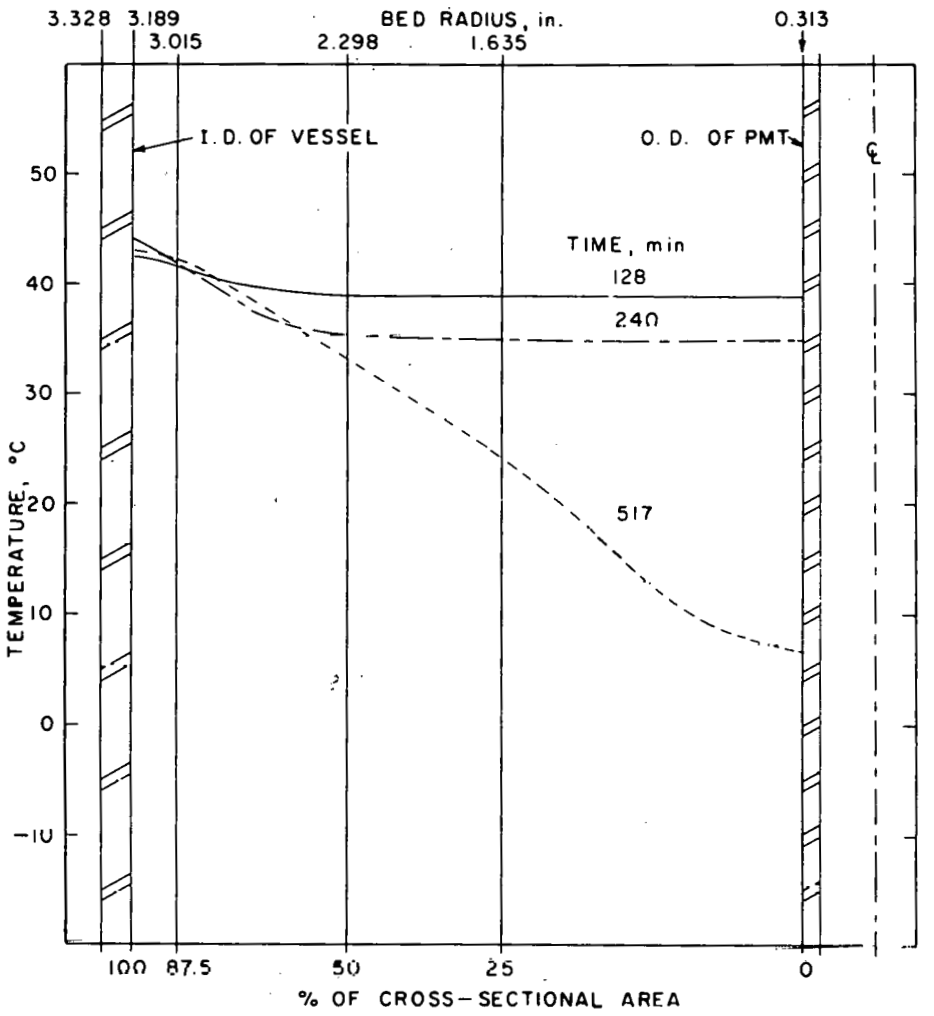

Figure 33. Analytical temperature profiles for Run E08D1.